

# Algorithmic detection of the crystal structures from three-dimensional real-space analysis

Sumitava Kundu,<sup>1</sup> Kaustav Chakraborty,<sup>1</sup> and Avisek Das<sup>1</sup>

*School of Chemical Sciences, Indian Association for the Cultivation of Science,  
Kolkata, India, 700032*

(\*Electronic mail: mcsad@iacs.res.in)

(Dated: 15 July 2024)

Crystal structure detection from the real-space analysis only is still a big challenge in multiple disciplines due to the absence of exact analytical or computational methods. New types of complex crystal structures seek more involvement of advanced techniques and understandings as well as developing new kinds of machinery. Despite the existence of proper experimental techniques of crystal structure detection, it lacks the exact approach to obtain the complete unit cell information from the three dimensional coordinates only. In this research, we propose an exact prescription to detect the crystal structures in real-space based on the arrangements of the local environment and by searching for the directions of possible translational vectors. The protocol yields good agreements with the experimental results for any simple or complex crystal structures irrespective of the single-component or multi-component systems allowing the complete execution to take a minimal time and computational cost. To the best of our knowledge, this algorithmic prescription can be applied to detect the unit cell of crystal structure and identify the space group across the domains of condensed matter physics and material sciences.

## I. INTRODUCTION

Crystal or crystalline solid is the periodic arrangement of constituents (atoms, molecules, ions etc.) that extends in all directions<sup>1</sup>. The detection of crystal structure has been investigated over the last century in many theoretical or experimental studies and still intriguing in nature across multiple disciplines of science. X-ray diffraction method was proposed for more than hundred years ago<sup>2-5</sup>, which became the most useful and versatile technique to detect the crystal structure experimentally<sup>6,7</sup>. In experiments, the positions and intensities of the Bragg peaks are measured via X-ray<sup>4,8-11</sup>, which is one of the most used approaches to solve the crystal structure currently. Later, the scattering of neutrons<sup>11</sup> and electrons<sup>10,12,13</sup> were also introduced depending on the scientific demands. This data is further fed to a computer program<sup>14-16</sup> to determine the unit cell parameter and space group by analyzing the properties of the Fourier transform<sup>17-26</sup>. The reciprocal lattice arises from the Fourier transform of another direct or real lattice, which is a periodic arrangement of atoms or molecules in real space. These formulations are based on the theory of reciprocal space and it is mostly used in experiments to handle the detection of crystal structure. The structures of ionic crystals<sup>27</sup>, electronic crystals<sup>28</sup>, metallic crystals<sup>29-31</sup>, nanocrystal superlattices<sup>32-36</sup> etc. were observed in experiments. Very recently, a direct approach of identifying the ionic colloidal crystal structures was proposed in three dimensional real-space by matching the index of fluorescently labelled particles and particle tracking<sup>37</sup>. Multiple experimental techniques have been developed to detect the crystal structures but surprisingly in computer simulations, one would face much more difficulties to identify the crystal structure completely, despite the access of all coordinates of the system in the real space, where as the crystal is a periodic arrangement of the coordinates. With the advancement of computer power, the investigation was started to study various scientific problems using the computer simulations such as, the phase transition of the solids, nucleation of the crystals etc. Identification of the crystal structure was important to solve these crucial problems which turned out to be a regular scientific exercise in the domain of computational material science or applied physics. The formation of the crystal structures using different kinds of idealized models i.e., hard particles<sup>38,39</sup>, patchy particles<sup>40,41</sup>, DNA-mediated nanoparticles<sup>42</sup> etc., were reported in the computer simulations<sup>43-47</sup>. But there was no straightforward approach to overcome this problem computationally till date; as a result the problem remains open

which demands a much more attention. The main challenge to detect the crystal structures from computer simulation is the system size and the equilibration times in the simulation are orders of magnitude smaller, which is still a huge barrier to identify the broken symmetry directions in three dimensions. The resolution and quality of numerical diffraction patterns are too poor to follow the standard protocol used in the experiments. So, the methods directly depending on the coordinates of the particles are required to serve the purpose.

A number of different routes based on the real-space analysis, were taken over the years to analyze the local order including the formation of order parameter based on the local neighbor<sup>48-52</sup>, common-neighbor analysis (CNA)<sup>49,53</sup>, templating<sup>54</sup>, graph analyses technique<sup>55,56</sup>. For the last few decades, the crystal structures has been detected computationally, but no straightforward and general approaches were pointed out in the literature. The Steinhardt order parameter which was actually developed to determine the symmetry of local neighbors in dense liquids using the spherical harmonics, is applicable to a very limited crystal structures such as Face-Centered Cubic (FCC), Body-Centered Cubic (BCC) or Hexagonal closed packed (HCP) crystals<sup>48</sup>. Recently, a large amount of local fingerprints data was used in machine learning algorithm<sup>57</sup> based on the detection of topology of the crystallographic environment<sup>58</sup>. The authors used the scale-free and rotation-invariant structural descriptors of a particle's local environment, which is sensitive to the symmetry of the local neighborhood. Their observation supports the detection of structural regions for complex structures but fails to point out the detail of a complex crystal structure. Artificial intelligence and deep learning algorithms also enhance the process of the determination of the crystal structures<sup>59</sup>. Recent developments can distinguish one complex structure from another<sup>58,60</sup>, but not capable of producing a particular crystallographic information without the references. Techniques have been developed to detect the crystal structures of chemical compounds based on the chemical spaces<sup>61,62</sup> or tuning the crystalline behavior in the interaction spaces<sup>63</sup>. In computer simulations, despite accessing all the coordinates of the constituents to measure radial distribution function (RDF), bond-orientational order (BOO) or diffraction pattern to decipher the signatures of crystal structures, no general routes were indicated towards the detection of crystal structures<sup>38,40,64-72</sup>. Different layers based on bond-orientational order (BOO) were developed to get more sensitive information of local neighbors but the approaches were restricted within few structures which did not serve the general purposes<sup>73-75</sup>. Recently, a theoretical approach was reported that analyses the point

group of the local neighbor directly from the particle coordinates and shed light on the paths towards the partial detection the crystal structures<sup>76</sup>. The rotational symmetry of the neighbor was detected, but it was unable to reveal the complete crystallographic symmetry and the space group, which remained as open problems. Considering the shortcomings of the former techniques, automatic identification of the crystal structure is still unsolved from the real-space analysis only.

In this research, we report a computational protocol to detect the unit cell and space group of the crystal structure using the three dimensional real-space analysis. Any other information except the particle coordinates were ignored to construct the formulation to detect the unit cell of the crystal structure. The basic difference of the Bravais and non-Bravais lattice is realized to convert a complex non-Bravais lattice into a Bravais one followed by the detection of the basis vectors of direct lattice considering the coordinates of the local neighbors. Based on a few widely used techniques developed to analyze the crystals, our approach works unambiguously for any crystal structures with simple or complex basis, beyond the single component systems and takes minimal time and computational cost. The approach uses minimum but necessary information in the real space i.e., the coordinates of the particles only, in order to detect the unit cell and space group which involves the standard computational “neighbor-search” algorithm in different ways by minimizing the possibilities step-by-step. Each and every step of the protocol is presented using an example of ideal crystal structure with complex basis for the demonstration purpose. The prescription was applied to detect the unit cells and corresponding space groups of multiple synthetically prepared crystal structures without noise and the data seemed to agree well with the experimental results, which are reported here. We also applied the method on a complex crystal structure coming out of computer simulation and report the data along with the robustness of the approach at different noise levels. To the best of our knowledge, this is the first computational approach of its kind to identify the crystal structures of any ionic crystals, metallic crystals or covalent network crystals etc. in the real-space which can be useful in a wider community of condensed matter physics, applied physics or material sciences.

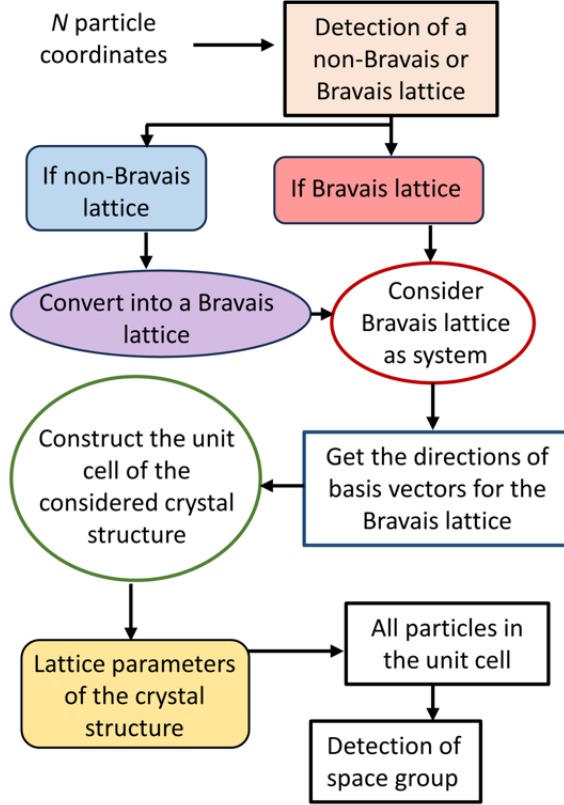


FIG. 1. A schematic diagram of the important steps of protocol is shown.

## II. METHODS

The coordinates of all particles in a crystal structure are defined in real-space. An unit cell is defined as a combination of both the basis vectors and effective coordinates of the basis that can be replicated to construct the entire crystal structure by translations only. In three dimensional system, a crystal structure can be classified into seven crystal classes and fourteen Bravais lattices within 230 space groups. For a crystal class, the translational vectors can be different from the primitive lattice vectors which are constructed by the joining vectors to the adjacent particles. It is well known that a primitive unit cell is the smallest volume formed by the primitive lattice vectors which contains only one effective particle inside the cell. For any primitive Bravais lattice, the basis vectors coincide with the primitive lattice vectors. A non-primitive Bravais unit cell consists of more than one effective particles, which are also called “centered unit cell”. As the choice of the unit cell is not unique for a crystal structure, there exists multiple possible basis vectors corresponding to the unit cells in different crystal classes. It follows that one particular crystal class may

include multiple choices of basis vectors depending on the crystal structure where all the choices are valid for the crystal structure until a particular choice violates an allowed Bravais unit cell under the corresponding crystal class. An allowed Bravais unit cell refers to a valid unit cell defined in a crystal class. For example, a “base-centered” unit cell is not allowed in the cubic class, hence it is not a rational choice. So, it is important to find out the crystal class and right choices of basis vectors leading to the allowed Bravais lattice in that class for the entire crystal.

As we are not interested in identifying the primitive unit cell of the crystal structure only, we try to evaluate the allowed directions of the basis vectors for a Bravais unit cell corresponding to the crystal class. If the considered structure does not satisfy the requirement of Bravais lattice, a transformation into the Bravais lattice (either primitive or non-primitive) is required. The key difference between a Bravais and non-Bravais lattice is, all the particles are equivalent for a Bravais lattice, which is not the case for a non-Bravais lattice<sup>1,77</sup>. In a non-Bravais lattice, all the particles are non-equivalent, confirming the existence of multiple types of environment present in the system. This fundamental difference is exploited to detect a system whether it is Bravais or non-Bravais in nature. If the considered structure is a non-Bravais one, at first the system is transformed into a Bravais system and the directions of basis vectors are identified using the coordinates of the particles in the Bravais lattice only as discussed in the following sections. Then the unit cell parameters are detected and the identification of all particles are done followed by the determination of the space group of the crystal structure. The primary steps of the methodology are as follows.

1. Environment detection of the system and separation of the environment if non-Bravais lattice
  - Evaluation of the radial distribution function (RDF) and the positions of the local neighbors within a certain distance.
  - Determination of the number of clusters formed by the neighbors in presence of statistical noise and the centroid of the clusters using standard *K-Means* clustering method<sup>78</sup> and separation of the particles with similar environment.
  - Bravais lattice if all particles have similar kind of environment, otherwise non-Bravais lattice. If non-Bravais lattice, transform the system into a Bravais lattice.

2. Considering the Bravais lattice as the system, detection of crystal class : all possible directions of vectors
  - Construction of a convex polyhedron using the centroid of the clusters of the distribution of local neighbors.
3. Evaluation of the set consisting of the directions of all possible basis vectors for the Bravais lattice under the crystal class
4. Construction of the unit cell of considered crystal structure for each choice of basis vectors satisfying Bravais unit cell
5. Determination of the space group of the crystal structure

A schematic diagram of the approach is shown in Fig.1 indicating all the primary and necessary steps starting from the consideration of the particle coordinates of the system up to the determination of the unit cell and space group of a crystal structure. The steps are elaborated to accomplish the detection of the crystal structure using the ideas plugged into the course. To demonstrate the mechanism of the approach, a synthetically prepared ideal system of  $\beta$ -Mn crystal was used with lattice parameters  $a=6.315$ ,  $b=6.315$ ,  $c=6.315$ ,  $\alpha=90^\circ$ ,  $\beta=90^\circ$ ,  $\gamma=90^\circ$  and space group  $P4_132$ , which was verified experimentally<sup>9</sup>. The unit cell of the  $\beta$ -Mn crystal consisting of twenty particles (without any noise) was chosen to replicate in the three dimensions, resulting an ideal  $\beta$ -Mn crystalline system, as shown in Fig.2A. We used only the coordinates of the particles and any other information was lost intentionally. Our final goal was to get one of the right choices of basis vectors and unit cell back for the crystal structure.

### **A. Detection and separation of the environment : Bravais or non-Bravais lattice and conversion of a non-Bravais lattice into a Bravais lattice**

As the first step of the scheme, a crystal structure is checked whether it is a Bravais lattice or not. The configuration shown in Fig. 2A is chosen as the system of the interest and the position of all particles are accessed in three-dimensional Cartesian coordinate system. We detect types of the positional environment for all particles in the system and separate the

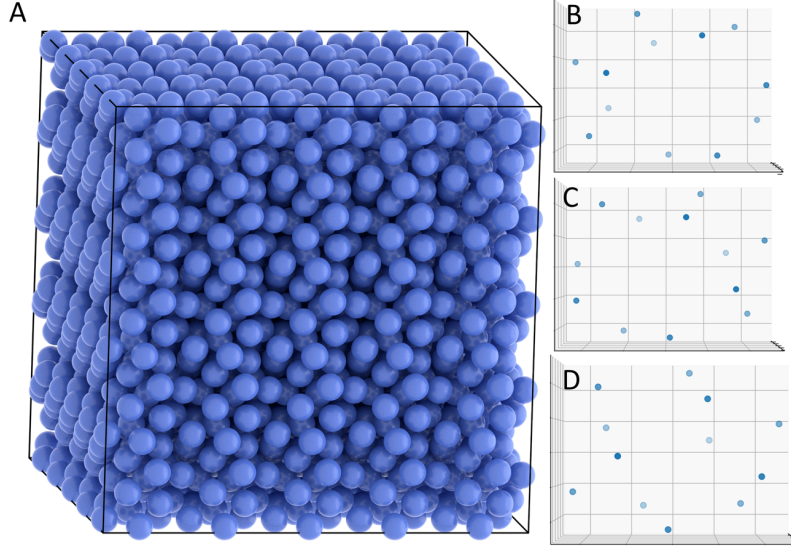


FIG. 2. (A) An ideal system of  $\beta$ -Mn crystal is shown. (B) The distributions of neighbors within the distance  $r_c \sim 2.6$  were considered for three arbitrarily chosen particles from the crystal structure, showing completely different kind of distributions for the particles.

particles sharing similar environment following a technique namely “environment separation” which is as described below.

In principle, the environment of a particle can be realized by the positional distribution of the neighbor particles around itself. A simple protocol includes choosing a particle from the system randomly followed by the observation of the distribution of the neighbor particles around itself within a certain distance. Subsequently, multiple kinds of environment correspond to the existence of different kinds of positional distribution of the neighbors around the particles in the system estimated within the fixed distance. So, a simple realization is that if there exists more than one kind of positional arrangement of the neighbors for all the particles in the system within a fixed distance, the system is said to be a non-Bravais lattice. If all the particles have similar kind of distribution of the neighbors, the system is Bravais in nature as all the particles in the system are equivalent. For the instance, a system of ideal  $\beta$ -Mn crystal structure is showcased in Fig. 2A. The positional distributions of the neighbors within a certain distance ( $\sim 2.6$ ) for all particles in the system were obtained upon performing a simple “neighbor search” calculation using *freud-toolkit*<sup>79</sup>. We observed multiple kind of distributions of the neighbors and the distributions for only three arbitrarily chosen particles from the system are shown in Figs. 2B, C, D for the demonstration purpose.



Only visual inspection confirms that the three randomly selected particles have different kinds of environment without further quantitative data. An obvious statement can be made that more than one kind of environment exists in the system of  $\beta$ -Mn crystal; so the system is a non-Bravais lattice. As we understand that only visual inspection is not enough to detect the types of the environment if the system is more complex or noisy; we need to use a general and robust algorithmic approach to detect the environment. As the output of this scrutiny, a system is said to be either Bravais or non-Bravais lattice.

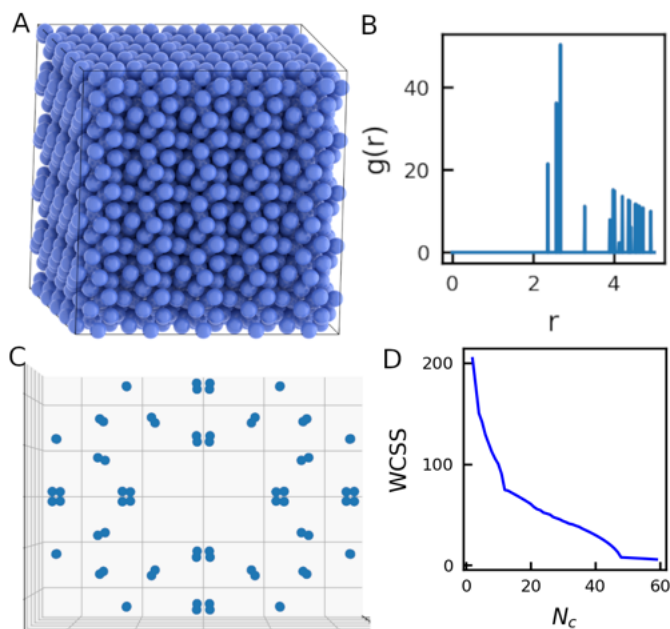


FIG. 3. (A) An ideal system of  $\beta$ -Mn crystal (complex basis) and the corresponding RDF (B) is shown. Detecting the first minimum, i.e. nearest neighbor distance  $\sim 2.6$ , (C) the position of the atoms within  $r_c$  has been evaluated confirming eight unique clouds of particles from *K-Means* clustering as shown in (D).

For a non-Bravais lattice, the “environment separation” technique is decomposed into two sub-categories, (i) positional distribution of the local neighbors of all particles in the system and (ii) separation of the particles based on the unique environments after clustering the points of the three dimensional distribution of the neighbors. These steps are explained below in detail.

## 1. Positional distribution of the local neighbors

As a part of the “environment detection” technique, at first it is required to know the positional distribution of the local neighbors of all particles in the system. We consider a system with  $N$  particles. The radial distribution function (RDF) is evaluated considering the geometric centers of particles measuring the normalized particle density as a function of distance from a central particle as shown in Fig. 3B using the *freud*-toolkit<sup>79</sup>.  $N_{CN}$  is the number of neighbors for each particle within the distance,  $r_c$ , which is chosen to be a minima of RDF. In general the first minima of RDF is preferred to calculate the positional distributions of the nearest neighbors in three dimensions. For this example,  $r_c$  was chosen as 2.6 and  $N_{CN}$  appeared to be 13. All the pairwise position vectors of the particles are calculated within the distance  $r_c$ , using  $\vec{r}_{ij} = \vec{r}_j - \vec{r}_i$ , where  $i \in (0, N)$  and  $j \in (0, N_{CN})$  for particle  $i$ , followed by the superposition of all vectors  $\vec{r}_{ij}$ . This gives the overall positional arrangement of all the neighbors for all the particles in the system, which can be considered as the bond orientational order (BOO) of the system in three dimensions, as shown in Fig. 3C. For an ideal crystal, a distribution of the particles with zero positional deviation is obtained but in real simulation data, few cluster of particles are observed with statistical noise, located at the distance  $\sim r_c$ , due to the translational symmetry of the crystal structure.

## 2. Clustering and environment detection

The number of clusters ( $N_c$ ) is calculated using the *K-Means* clustering method<sup>78</sup> by detecting the elbow of the two-dimensional plot of the sum of the square distance between particles in a cluster and the cluster centroid (WCSS stands for “Within-Cluster Sum of Square”) versus k-value (*x-axis*) as the standard approach, as shown in Fig. 3D. The elbow is determined as a number in the *x-axis* after which, the value of WCSS decreases almost monotonically. The centroid of  $N_c$  clusters are evaluated with the positions around the centre (0, 0, 0). For an ideal system, the centroid of the clusters are not required to calculate due to the absence of any positional fluctuations as in the real system leading to the coordinate of the centroid of a cluster coinciding with the points. But in real simulation data, the identification of the clusters is important followed by the determination of the centroid of the clusters. For ideal  $\beta$ -Mn structure,  $N_c$  ( $\neq N_{CN} = 13$ ) was 48 as shown in the elbow

analysis (Fig. 3D). Additionally, the cluster ids of all  $\vec{r}_{ij}$  vectors in the bond order diagram are identified to know the environment of all the particles in the system.

The environment of a particle  $i$  is characterized by the cluster ids of neighbors around itself within a distance  $r_c$ .  $\zeta$  corresponds to the environments of all particles in the system and  $\zeta_{im}$  indicates the cluster id of  $m$ -th neighbor of  $i$ -th particle, where  $i \in (0, N)$  and  $m \in (0, N_{CN})$  within  $r_c$  distance. So  $\zeta_i$  refers to the set of cluster ids of all  $N_{CN}$  neighbors of  $i$ -th particle. As multiple particles can possess similar environment in a crystal structure, we find the particles with similar type of environment i.e., unique  $\zeta_i$  based on the integer values (cluster ids of all neighbors) by varying  $i$  from 0 to  $N$  consecutively. For example, if  $\zeta_1$  and  $\zeta_2$  defining the cluster ids of the neighbors of particle 1 and 2 respectively, share identical values then these two particles are said to have similar environment in an ideal system. From the system, unique  $\zeta_i$ s are sorted out and total number of unique  $\zeta_i$  is a quantification of the types of environment for all particles in the system. The particle ids having identical  $\zeta_i$  (any one among the unique  $\zeta_i$ s) are identified and total number of such particles sharing similar environment is denoted by  $N_s$ . If the initial system is an ideal Bravais lattice then all  $\zeta_i$  are identical i.e.,  $N_s = N$ , as all particles in a Bravais lattice share similar kind of environment and those are equivalent. In the simulated system,  $N_s$  becomes almost comparable with  $N$ ;  $N_s \sim N$ , due to the noise present in the system. In a non-Bravais lattice, as there exists multiple types of environment,  $N_s$  is very less than  $N$  confirming the existence of more than one unique  $\zeta_i$  for all the particles. The formulation indicates that  $N_{CN} \leq N_c$  where  $N_{CN}$  is the number of neighbors of each particle in the system within  $r_c$  and  $N_c$  corresponds to the total number of clusters formed by all particles in the system. For a non-Bravais lattice, more than one kind of environment suggests the presence of extra clusters than that of a Bravais lattice, as all particles in the Bravais system share similar environment following the number of clusters  $N_c$  of all particles to be equal with  $N_{CN}$ . Following the recipe, the decision can be made by comparing the number  $N_s$  with  $N$  barring the noise; if  $N_s \sim N$ , the system is called a Bravais system, otherwise it is a non-Bravais one. For the ideal  $\beta$ -Mn system shown in Fig. 2A, total number of environments appeared to be twenty for all particles in the system within the distance  $r_c = 2.6$ .  $N_s$  was found to be very less than  $N$  ( $N_s = 0.05 \times N$ ) indicating the existence of multiple types of environment confirming the system as a non-Bravais lattice. Figs. 2B, C, D also suggest the existence of different kinds of environment for three arbitrarily chosen particles from the

ideal  $\beta$ -Mn system, where the local neighbors of the particles within the distance  $r_c$  were shown separately in each sub-figure.

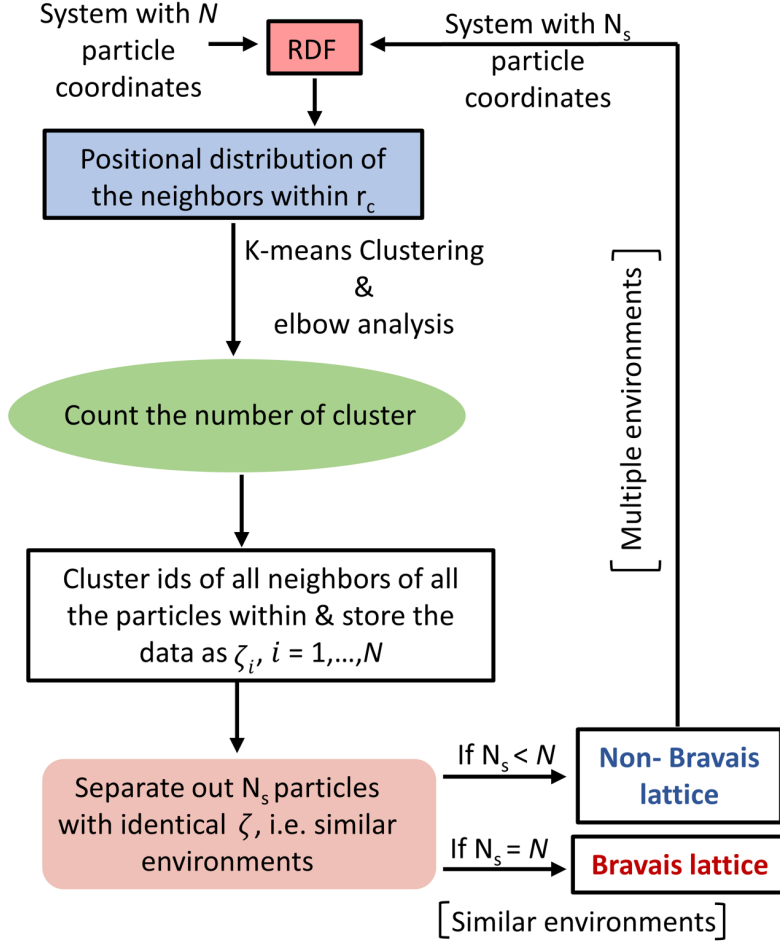


FIG. 4. The schematic diagram of the “environment separation” technique is shown

### 3. *Environment separation of a non-Bravais lattice*

If the initial structure appears to be a non-Bravais lattice, it is compulsory to perform the “environment separation” technique to transform the non-Bravais system into a Bravais one, which is not an essential requirement if the initial system is a Bravais lattice. To perform the “environment separation”, we need to consider an updated system with  $N_s$  particle coordinates only, which are obtained upon separating the  $N$  particles in the initial system based on the environments. This does not necessarily mean that all the  $N_s$  particles in the transformed system will have similar kind of environment around themselves, when only  $N_s$

particles are considered as the system. For the confirmation check the coordinates of the  $N_s$  particles are considered as the transformed system (total number of particle in the updated system is  $N_s$  i.e.,  $N = N_s$ ) and all the previous steps consisting of the calculation of RDF, BOO, *K-Means* clustering are applied sequentially again, followed by the categorization of particles based on the updated environments and separation of the  $N_s$  particles with similar kind of environment. If  $N_s = N$ , the system is transformed into a Bravais lattice, but if not then the protocol needs to be performed again. So, this process is performed in an iterative way and at each step of the iteration, the coordinates of  $N_s$  particles coming out of the previous environment separation are considered as the transformed system until all the particles in the transformed system have similar kind of environment. The iteration for the “environment separation” process discontinues if the number of particles having similar kind of environment matches with the number of particles considered as the system at the start of that particular step of iteration barring the noise. The transformed Bravais lattice does not necessarily required to be a primitive cell. The schematic diagram of the “environment separation” technique is shown in Fig. 4 and the number of iteration for the separation protocol depends on the number of environments present in the initial system within the distance  $r_c$ . For a non-Bravais lattice, the system changes into a Bravais lattice after performing all the required steps; while Bravais lattice remain unchanged, which eventually does not require any conversion. In principle, a Bravais lattice can always be extracted from a non-Bravais lattice irrespective of the existence of multiple kinds of environment present in the system. The algorithmic representation of the “environment separation” technique is described below.

---

**Require:**  $N$  particle coordinates

RDF

BOO within  $r\_c$

*K-Means* clustering with local neighbors

Calculate  $\zeta$  for all particles

Separate  $N_s$  particles based on  $\zeta_i$ , where  $i \rightarrow 0, N$

**while**  $N_s < N$  **do**

$N \leftarrow N_s$  (Update  $N$ )

    Updated system with  $N$  particles

    RDF

    BOO within  $r\_c$

*K-Means* clustering with local neighbors

    Calculate  $\zeta$  for all particles in the updated system

    Separate  $N_s$  particles based on  $\zeta_i$ , where  $i \rightarrow 0, N$

**end while**

---

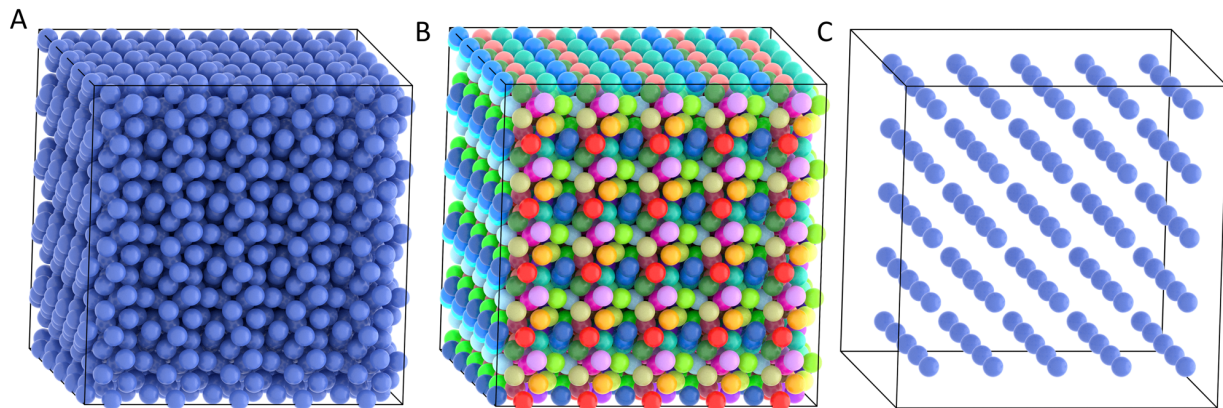


FIG. 5. (A) An ideal system of  $\beta$ -Mn crystal, (B) the same system with atoms in multiple colors based on the similar kind of environment and (C) a reduced Bravais lattice after environment separation are shown.

After the detection of the environment, the “environment separation” method is performed in the iterative way if required; a non-Bravais lattice converts into a Bravais lattice, as the complex  $\beta$ -Mn crystal transforms into a “simple cubic” lattice within a single iteration as shown in Fig. 5. For this example, the transformation of a non-Bravais lattice into a

primitive Bravais lattice does not necessarily mean that the transformation will always occur in primitive Bravais lattice like the  $\beta$ -Mn structure; in principle, the transformation may convert a non-Bravais lattice into any of the fourteen Bravais lattices. The  $\beta$ -Mn crystal structure is shown with the particles in single color (Fig. 5A), followed by the categorization of the particles based on the environments as shown in Fig. 5B, indicating the particles with similar environment in the same color. The particles with any particular color (for example, the particles in “blue” color) are chosen and considered as the system for further analysis. The choice of the particular set of particles does not depend on the type of the Bravais lattice; any particular choice satisfies the same Bravais lattice. It is important to note, the chosen coordinates of the particles with similar environment are already present in the initially considered non-Bravais  $\beta$ -Mn crystal structure and our goal is to find those particles following the protocol described above.

## B. Identification of crystal class and all possible directions

In this subsection, our aim is to get the directions of all possible vectors,  $\hat{\mathbf{a}}_d$ ,  $\hat{\mathbf{b}}_d$ ,  $\hat{\mathbf{c}}_d$ , which can be considered as one of the possible choices of the basis vectors. In general, all the possible choices may not be valid as some of those fail to produce the allowed Bravais lattices among fourteen, defined under one of the seven crystal classes. The transformed Bravais lattice (here, “simple cubic” lattice for  $\beta$ -Mn structure) is considered as the system for the time being and used in next few steps. This approach to identify the crystal class is decomposed into further sub-categories; the construction of a convex polyhedron using the centroid of the clusters in the BOO after the *K-Means* clustering and evaluation of all possible directions from the polyhedron.

### 1. Construction of convex polyhedron from the positional distribution of all neighbors

The transformed Bravais lattice is considered as the reduced structure and the system of interest, which is used to evaluate the positional distribution of the local neighbors. We perform exactly similar analyses including the determination of RDF (Fig. 6A) with a further selection of the first minimum of the RDF,  $r_c \sim 6.5$ . The pairwise position vectors  $\vec{r}_{ij}$  are

calculated using the coordinates of the particles producing a completely different type of positional distribution for the “simple cubic” Bravais lattice as shown in Fig. 6B.

After applying the *K-Means* clustering method on the positional distribution, the number of clusters turns out to be  $N'_c$  ( $= 6$  for this example as shown in Fig. 6C). The centroid of the  $N'_c$  clusters is further used to construct a convex polyhedron. A similar approach was reported earlier in the context of crystal structure detection by matching the templates of the local neighbors<sup>80</sup>. In this example, the constructed polyhedron is an Octahedron with six vertices as shown in Fig. 6D. The constructed polyhedron may not be regular always, but must have the property of convexity. For the simulated system with noise, the constructed polyhedron can not be a regular one, but the convexity always remains there within the tolerances.

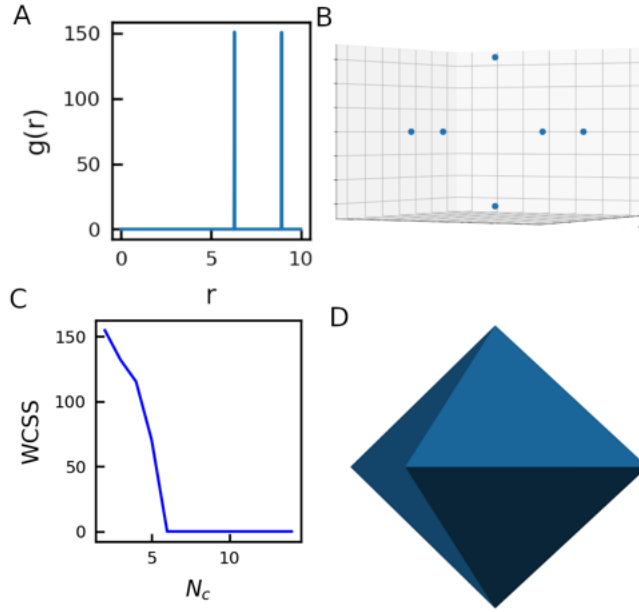


FIG. 6. (A) The RDF, (B) BOO are shown for the Bravais lattice. The number of clusters is six as confirmed by the elbow analysis of *K-Means* clustering (C), and (D) constructed convex polyhedron using the centroid of the clusters are shown.

## 2. Evaluation of all possible directions from the polyhedron

For any of the fourteen Bravais lattices, the directions of the three lattice vectors i.e.  $\hat{\mathbf{a}}_d$ ,  $\hat{\mathbf{b}}_d$ ,  $\hat{\mathbf{c}}_d$  appear to intersect either any vertices, or face mid-points or edge mid-points



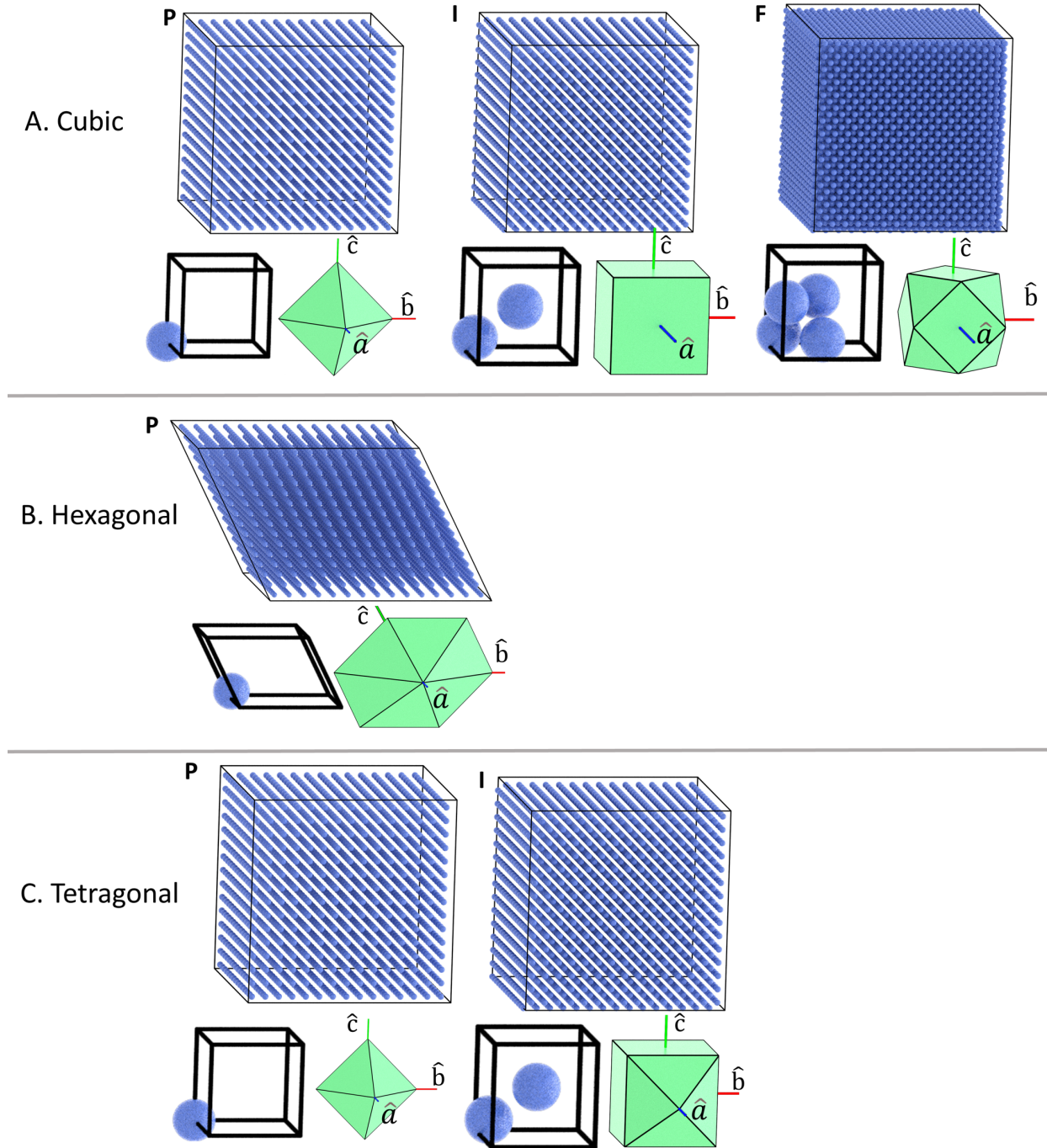


FIG. 7. Synthetically prepared crystal structures of the Bravais lattices corresponding to (A) Cubic, (B) Hexagonal and (C) Tetragonal classes are shown. The corresponding unit cells of the structures and the convex polyhedra constructed from the distribution of the local neighbors along with the directions of the lattice vectors,  $\hat{a}$ ,  $\hat{b}$ ,  $\hat{c}$  are displayed for each case. The letters **P**, **I**, **B**, **F** designate the primitive, body-centered, any base-centered and all face-centered Bravais unit cell respectively for each crystal class.

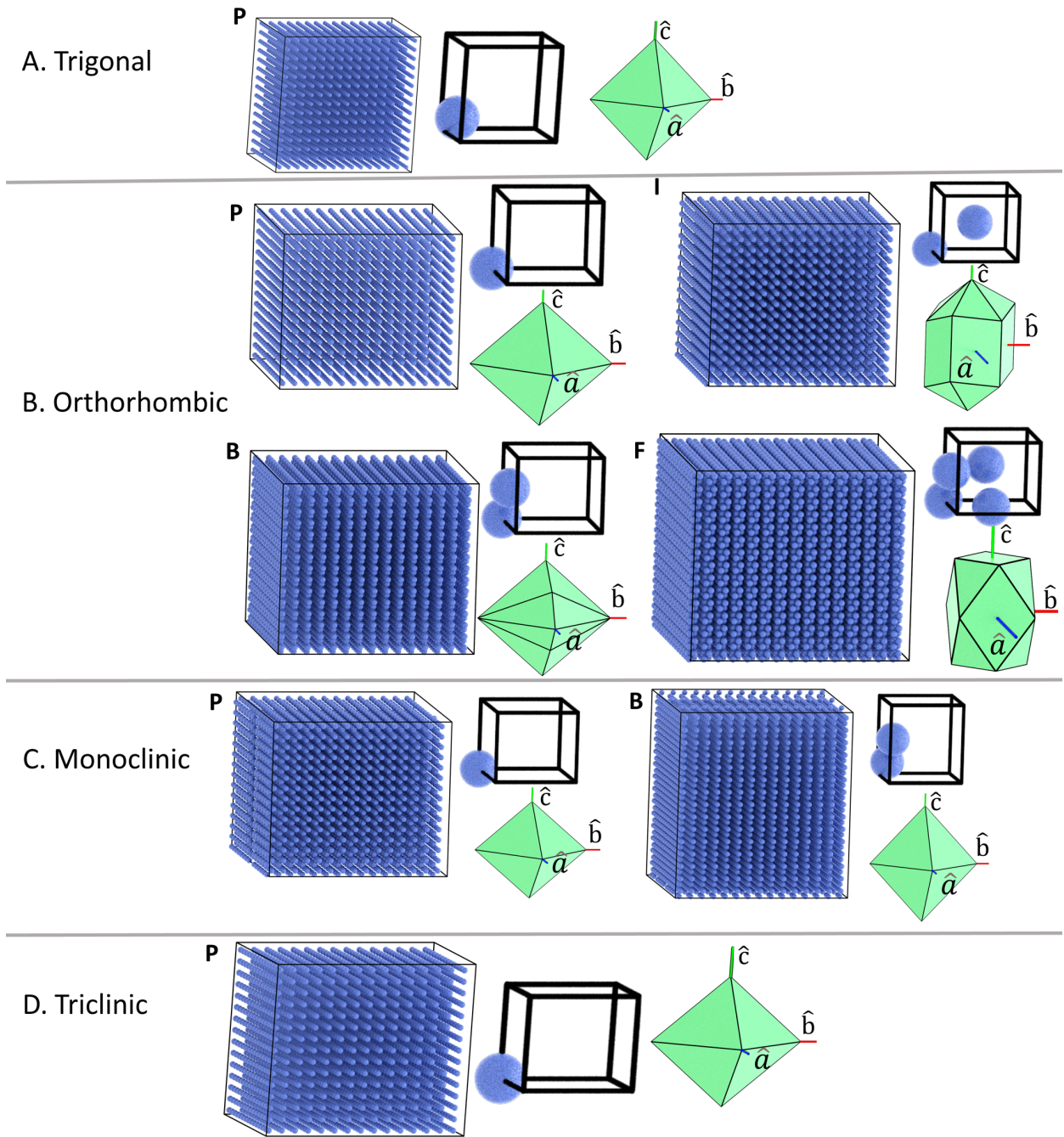


FIG. 8. Synthetically prepared crystal structures of the Bravais lattices corresponding to (A) Trigonal, (B) Orthorhombic and (C) Monoclinic and (D) Triclinic crystal classes are shown. The corresponding unit cells of the structures and the convex polyhedra constructed from the distribution of the local neighbors along with the directions of the lattice vectors,  $\hat{a}$ ,  $\hat{b}$ ,  $\hat{c}$  are displayed for each case. The letters **P**, **I**, **B**, **F** designate the primitive, body-centered, any base-centered and all face-centered Bravais unit cell respectively for each crystal class.

of the polyhedron constructed with the centroid of the neighbors of the Bravais lattice as shown in Figs. 7, 8. The polyhedron may change depending on the distance  $r_c$  considered to calculate the neighbors, but the directions of the lattice vectors always intersect either any of the vertices or face-midpoints or edge-midpoints. It follows that if the Bravais lattice is a primitive unit cell with only one effective particle per unit cell, the directions of the basis vectors intersect any of the vertices of the constructed polyhedron. In principle, the directions of rotational symmetry axes of the polyhedron point group can be considered for the structures with crystal class of higher symmetries but this consideration is not effective for the crystal classes with lower number of rotational symmetry like Monoclinic or Triclinic. In order to calculate the face mid-points and edge mid-points of the polyhedron, the *convex-decomposition* technique of *Coxeter* toolkit is used<sup>81</sup>. The vertices, forming each face and edge are determined followed by the calculation of the geometric centres of the faces and edge mid-points. The coordinates of all the vertices, face-midpoints and edge-midpoints are known around the center of the constructed polyhedron and all the joining vectors are non-unit vectors.  $g$  is the total number of joining vectors passing through any of these attributes of polyhedron with origin at  $(0, 0, 0)$  and all the vectors are considered for the determination of the direction of lattice vectors.

Each triplet of the  ${}^gC_3$  combinations is considered as a set of  $\vec{\mathbf{a}}_d, \vec{\mathbf{b}}_d, \vec{\mathbf{c}}_d$  and used to detect the crystal class among seven, by measuring the  $|\vec{\mathbf{a}}_d|, |\vec{\mathbf{b}}_d|, |\vec{\mathbf{c}}_d|$  and the mutual angles defined as  $\alpha, \beta$  and  $\gamma$  within a distance ( $\mathcal{X}_d$ ) and angle ( $\mathcal{X}_a$ ) tolerance for the real system (for an ideal system,  $\mathcal{X}_d=0$  and  $\mathcal{X}_a=0$ ). The seven crystal classes are considered according to the order of the crystallographic point group symmetry; cubic (48), hexagonal (24), tetragonal (16), trigonal (12), orthorhombic (8), monoclinic (4) and triclinic (2). Each triplet consisting of three non-unit vectors, is checked computationally to satisfy the criteria of any of the crystal classes. The necessary conditions of satisfying the seven crystal systems based on the lattice parameters  $|\vec{\mathbf{a}}_d|, |\vec{\mathbf{b}}_d|, |\vec{\mathbf{c}}_d|, \alpha, \beta, \gamma$  are discussed below.

1. Cubic  $\rightarrow$   $||\vec{\mathbf{a}}_d| - |\vec{\mathbf{b}}_d|| \leq \mathcal{X}_d, ||\vec{\mathbf{a}}_d| - |\vec{\mathbf{c}}_d|| \leq \mathcal{X}_d, ||\vec{\mathbf{b}}_d| - |\vec{\mathbf{c}}_d|| \leq \mathcal{X}_d, |\alpha - \beta| \leq \mathcal{X}_a, |\gamma - \beta| \leq \mathcal{X}_a, |\alpha - \gamma| \leq \mathcal{X}_a, (90^\circ - \mathcal{X}_a) \leq \alpha \leq (90^\circ + \mathcal{X}_a), (90^\circ - \mathcal{X}_a) \leq \beta \leq (90^\circ + \mathcal{X}_a), (90^\circ - \mathcal{X}_a) \leq \gamma \leq (90^\circ + \mathcal{X}_a)$
2. Hexagonal  $\rightarrow$  (i)  $||\vec{\mathbf{a}}_d| - |\vec{\mathbf{b}}_d|| \leq \mathcal{X}_d, ||\vec{\mathbf{a}}_d| - |\vec{\mathbf{c}}_d|| > \mathcal{X}_d, ||\vec{\mathbf{b}}_d| - |\vec{\mathbf{c}}_d|| > \mathcal{X}_d, (90^\circ - \mathcal{X}_a) \leq \alpha \leq (90^\circ + \mathcal{X}_a), (90^\circ - \mathcal{X}_a) \leq \beta \leq (90^\circ + \mathcal{X}_a), (120^\circ - \mathcal{X}_a) \leq \gamma \leq (120^\circ + \mathcal{X}_a)$

$$(ii) \|\vec{a}_d\| - \|\vec{c}_d\| \leq \mathcal{X}_d, \|\vec{a}_d\| - \|\vec{b}_d\| > \mathcal{X}_d, \|\vec{b}_d\| - \|\vec{c}_d\| > \mathcal{X}_d, (90^\circ - \mathcal{X}_a) \leq \alpha \leq (90^\circ + \mathcal{X}_a), \\ (120^\circ - \mathcal{X}_a) \leq \beta \leq (120^\circ + \mathcal{X}_a), (90^\circ - \mathcal{X}_a) \leq \gamma \leq (90^\circ + \mathcal{X}_a)$$

$$(iii) \|\vec{b}_d\| - \|\vec{c}_d\| \leq \mathcal{X}_d, \|\vec{a}_d\| - \|\vec{b}_d\| > \mathcal{X}_d, \|\vec{a}_d\| - \|\vec{c}_d\| > \mathcal{X}_d, (120^\circ - \mathcal{X}_a) \leq \alpha \leq (120^\circ + \mathcal{X}_a), \\ (90^\circ - \mathcal{X}_a) \leq \beta \leq (90^\circ + \mathcal{X}_a), (90^\circ - \mathcal{X}_a) \leq \gamma \leq (90^\circ + \mathcal{X}_a)$$

3. Tetragonal  $\rightarrow \rightarrow$  (i)  $\|\vec{a}_d\| - \|\vec{b}_d\| \leq \mathcal{X}_d, \|\vec{a}_d\| - \|\vec{c}_d\| > \mathcal{X}_d, \|\vec{b}_d\| - \|\vec{c}_d\| > \mathcal{X}_d, |\alpha - \beta| \leq \mathcal{X}_a, \\ |\gamma - \beta| \leq \mathcal{X}_a, |\alpha - \gamma| \leq \mathcal{X}_a, (90^\circ - \mathcal{X}_a) \leq \alpha \leq (90^\circ + \mathcal{X}_a), (90^\circ - \mathcal{X}_a) \leq \beta \leq (90^\circ + \mathcal{X}_a), \\ (90^\circ - \mathcal{X}_a) \leq \gamma \leq (90^\circ + \mathcal{X}_a)$

$$(ii) \|\vec{a}_d\| - \|\vec{c}_d\| \leq \mathcal{X}_d, \|\vec{a}_d\| - \|\vec{b}_d\| > \mathcal{X}_d, \|\vec{b}_d\| - \|\vec{c}_d\| > \mathcal{X}_d, |\alpha - \beta| \leq \mathcal{X}_a, |\gamma - \beta| \leq \mathcal{X}_a, \\ |\alpha - \gamma| \leq \mathcal{X}_a, (90^\circ - \mathcal{X}_a) \leq \alpha \leq (90^\circ + \mathcal{X}_a), (90^\circ - \mathcal{X}_a) \leq \beta \leq (90^\circ + \mathcal{X}_a), \\ (90^\circ - \mathcal{X}_a) \leq \gamma \leq (90^\circ + \mathcal{X}_a)$$

$$(iii) \|\vec{b}_d\| - \|\vec{c}_d\| \leq \mathcal{X}_d, \|\vec{a}_d\| - \|\vec{b}_d\| > \mathcal{X}_d, \|\vec{a}_d\| - \|\vec{c}_d\| > \mathcal{X}_d, |\alpha - \beta| \leq \mathcal{X}_a, |\gamma - \beta| \leq \mathcal{X}_a, \\ |\alpha - \gamma| \leq \mathcal{X}_a, (90^\circ - \mathcal{X}_a) \leq \alpha \leq (90^\circ + \mathcal{X}_a), (90^\circ - \mathcal{X}_a) \leq \beta \leq (90^\circ + \mathcal{X}_a), (90^\circ - \mathcal{X}_a) \leq \\ \gamma \leq (90^\circ + \mathcal{X}_a)$$

4. Trigonal  $\rightarrow \|\vec{a}_d\| - \|\vec{b}_d\| \leq \mathcal{X}_d, \|\vec{a}_d\| - \|\vec{c}_d\| \leq \mathcal{X}_d, \|\vec{b}_d\| - \|\vec{c}_d\| \leq \mathcal{X}_d, |\alpha - \beta| \leq \mathcal{X}_a, \\ |\gamma - \beta| \leq \mathcal{X}_a, |\alpha - \gamma| \leq \mathcal{X}_a, \alpha \leq (90^\circ - \mathcal{X}_a) \text{ or } \alpha > (90^\circ + \mathcal{X}_a), \beta \leq (90^\circ - \mathcal{X}_a) \text{ or } \\ \beta > (90^\circ + \mathcal{X}_a), \gamma \leq (90^\circ - \mathcal{X}_a) \text{ or } \gamma > (90^\circ + \mathcal{X}_a)$

5. Orthorhombic  $\rightarrow \|\vec{a}_d\| - \|\vec{b}_d\| > \mathcal{X}_d, \|\vec{a}_d\| - \|\vec{c}_d\| > \mathcal{X}_d, \|\vec{b}_d\| - \|\vec{c}_d\| > \mathcal{X}_d, \rightarrow |\alpha - \beta| \leq \mathcal{X}_a, \\ |\gamma - \beta| \leq \mathcal{X}_a, |\alpha - \gamma| \leq \mathcal{X}_a, (90^\circ - \mathcal{X}_a) \leq \alpha \leq (90^\circ + \mathcal{X}_a), (90^\circ - \mathcal{X}_a) \leq \beta \leq (90^\circ + \mathcal{X}_a), \\ (90^\circ - \mathcal{X}_a) \leq \gamma \leq (90^\circ + \mathcal{X}_a)$

6. Monoclinic  $\rightarrow$  (i)  $\|\vec{a}_d\| - \|\vec{b}_d\| > \mathcal{X}_d, \|\vec{a}_d\| - \|\vec{c}_d\| > \mathcal{X}_d, \|\vec{b}_d\| - \|\vec{c}_d\| > \mathcal{X}_d, |\alpha - \beta| \leq \mathcal{X}_a, \\ |\gamma - \beta| \geq \mathcal{X}_a, |\alpha - \gamma| \geq \mathcal{X}_a, (90^\circ - \mathcal{X}_a) \leq \alpha \leq (90^\circ + \mathcal{X}_a), (90^\circ - \mathcal{X}_a) \leq \beta \leq (90^\circ + \mathcal{X}_a), \\ (90^\circ + \mathcal{X}_a) \leq \gamma$

$$(ii) \|\vec{a}_d\| - \|\vec{b}_d\| > \mathcal{X}_d, \|\vec{a}_d\| - \|\vec{c}_d\| > \mathcal{X}_d, \|\vec{b}_d\| - \|\vec{c}_d\| > \mathcal{X}_d, |\alpha - \gamma| \leq \mathcal{X}_a, |\gamma - \beta| \geq \mathcal{X}_a, \\ |\alpha - \beta| \geq \mathcal{X}_a, (90^\circ - \mathcal{X}_a) \leq \alpha \leq (90^\circ + \mathcal{X}_a), (90^\circ + \mathcal{X}_a) \leq \beta, (90^\circ - \mathcal{X}_a) \leq \gamma \leq (90^\circ + \mathcal{X}_a)$$

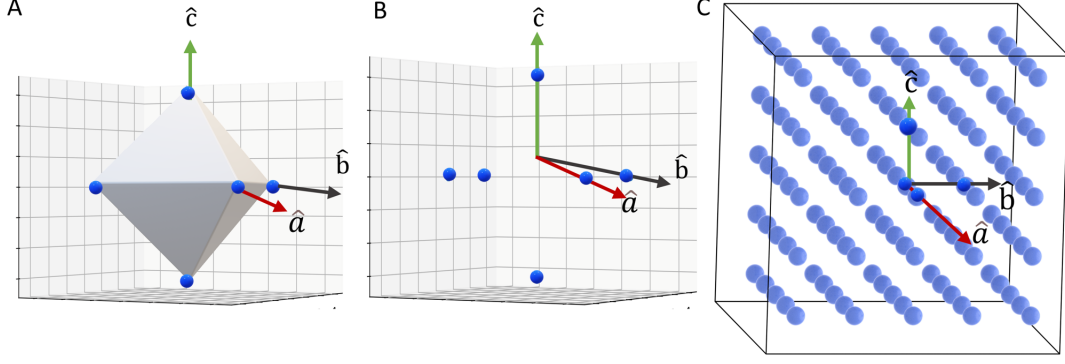


FIG. 9. (A) The direction of the lattice vectors  $\hat{a}$ ,  $\hat{b}$  and  $\hat{c}$ , passing through the vertices of the constructed Octahedron are shown. The coordinate of the neighbors without the Octahedron along with  $\hat{a}$ ,  $\hat{b}$  and  $\hat{c}$  as shown in (B), indicates the direction of lattice vectors as the valid choice of unit cell for the Simple Cubic Bravais lattice, displayed in (C).

$$(iii) \quad \|\vec{a}_d\| - \|\vec{b}_d\| > \mathcal{X}_d, \|\vec{a}_d\| - \|\vec{c}_d\| > \mathcal{X}_d, \|\vec{b}_d\| - \|\vec{c}_d\| > \mathcal{X}_d, |\beta - \gamma| \leq \mathcal{X}_a, |\gamma - \alpha| \geq \mathcal{X}_a, \\ |\alpha - \beta| \geq \mathcal{X}_a, (90^\circ + \mathcal{X}_a) \leq \alpha, (90^\circ - \mathcal{X}_a) \leq \beta \leq (90^\circ + \mathcal{X}_a), (90^\circ - \mathcal{X}_a) \leq \gamma \leq (90^\circ + \mathcal{X}_a)$$

$$7. \text{ Triclinic} \rightarrow \|\vec{a}_d\| - \|\vec{b}_d\| > \mathcal{X}_d, \|\vec{a}_d\| - \|\vec{c}_d\| > \mathcal{X}_d, \|\vec{b}_d\| - \|\vec{c}_d\| > \mathcal{X}_d, |\alpha - \beta| > \mathcal{X}_a, \\ |\alpha - \gamma| > \mathcal{X}_a, |\beta - \gamma| > \mathcal{X}_a$$

According to the observations, the crystal class of the Bravais lattice always involves the highest order crystallographic point group satisfied by the triplets from  ${}^gC_3$  combinations within the distance tolerance  $\mathcal{X}_d$  and angle tolerance  $\mathcal{X}_a$ . For example, if a system consists of triplets satisfying the cubic, tetragonal or monoclinic crystal classes, only those triplets corresponding to the cubic class are considered, as the cubic is of the highest order crystal class present in the system. All other triplets obeying lower symmetry crystal classes or no classes are ignored. We sort out those triplets corresponding to the highest order crystal class only which are considered as a set  $\mathcal{T}$  and used for further analysis. Multiple triplets corresponding to the same crystal class of the highest order can be present in the system depending on the crystal class. Each triplet of the set  $\mathcal{T}$  is capable of producing the entire Bravais lattice by translating a particle along each of the three directions. For the validation purpose in the ideal  $\beta$ -Mn system, we observed only one choice of the directions of the vectors, which was chosen as the directions of basis vectors by default. Those directions

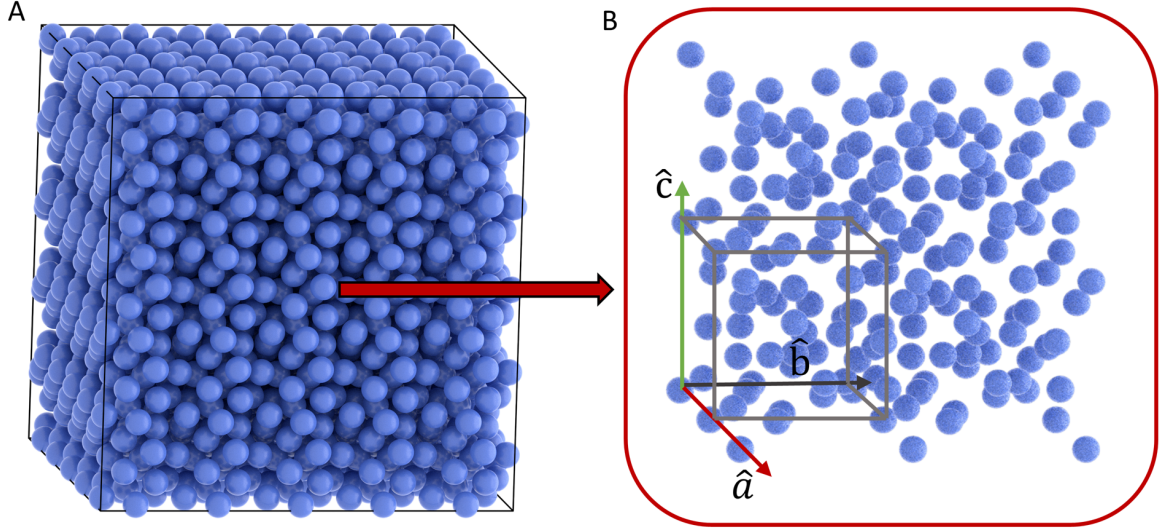


FIG. 10. (A) The non-Bravais lattice system with  $N$  particle coordinates are shown. (B) A random chunk of particles from the system are chosen and the direction of the lattice vectors,  $\hat{a}$ ,  $\hat{b}$  and  $\hat{c}$  are shown along with the unit cell for the validation purpose.

are shown in Fig. 9A with the constructed Octahedron using the particles in the BOO. The same particle coordinates of the neighbors in BOO are presented in Fig. 9B without the constructed polyhedron indicating the directions of the basis vectors to replicate the “simple cubic” (SC) Bravais lattice by translational only upon associating a random particle with a lattice site (Fig. 9C). This particular choice can be regarded as primitive lattice vectors because “simple cubic” is a valid Bravais unit cell in the cubic class, which is also a primitive cell. The particles shown in the deep “blue” color in Fig. 9C also supports the choice of the basis vectors. This choice is also valid even for the initial non-Bravais crystal structure as shown in Fig. 10.

The choices of the directions of the basis vectors do not depend whether these directions commensurate with the simulation box vectors or not, as the identification involves the local coordinate of the particles in the system. Though for this example, it is the case, but for a simulated system, this does not happen generally. The discussed methodology works well irrespective of this fact and does not get affected in the simulation data as well. One such example is discussed below as in the “Results” section.

### C. Identification of the directions of basis vectors of Bravais lattice

We consider the Bravais lattice and the triplets of set  $\mathcal{T}$  leading to the construction of the entire lattice. All the directions of triplets may not be the rational choices for the allowed Bravais unit cells (primitive or non-primitive) under the detected crystal class. So the directions of triplets satisfying the conditions are sorted out and those are the directions of basis vectors ( $\hat{\mathbf{a}}, \hat{\mathbf{b}}, \hat{\mathbf{c}}$ ). The detail protocol of separating all the directions of basis vectors from the set  $\mathcal{T}$  are discussed below.

#### 1. *Coordinates of the corner particles of the parallelepiped*

A triplet is chosen from the set  $\mathcal{T}$  and the directions of the triplet vectors are estimated followed by the association of a random particle from the Bravais lattice to a lattice site. The other corner particles of the parallelepiped are searched along each of the three directions of the considered vectors one by one in order to get the nearest particles. Association of a particle to a lattice site does not affect the space group of the crystal structure upon successful determination of the unit cell. This process helps us to get all the particles, located at the corners of the parallelepiped by searching the nearest one along a direction of the three lattice vectors as shown in cartoon figure (Fig. 11A).

Starting from a randomly chosen particle, say  $N_0$ , we get total four particles located at the corners of the parallelepiped,  $N_1, N_2, N_3$  at the minimum distances, joined via  $\hat{\mathbf{a}}, \hat{\mathbf{b}}, \hat{\mathbf{c}}$  respectively.  $N_4$  can be obtained by translating along  $\hat{\mathbf{c}}$  from  $N_1$ . The same protocol suggests,  $N_5$  is connected with  $N_3$  via  $\hat{\mathbf{b}}$  and  $N_6$  is attached with  $N_1$  via  $\hat{\mathbf{b}}$  at the minimum distances respectively as illustrated in Fig. 11A. The same figure also confirms that  $N_7$  is directly connected to  $N_6$  via  $\hat{\mathbf{c}}$ . In this way, the identities and coordinates of these eight corner particles of the parallelepiped are obtained. But the identities are not needed to be followed strictly as described here but one should stick to any particular representation for the rest of the approach. It should be noted that we use the transformed Bravais lattice system in case the initial system is non-Bravais in nature. Here, we identify the parallelepiped with eight corner particles, not the conventional Bravais lattice, which may or may not be a primitive cell. The algorithmic way to detect the eight corners of the parallelepiped is the following.

---

**Require:**  $\hat{a}, \hat{b}, \hat{c}$  and coordinates of all particles in Bravais lattice

$\mathcal{P} = []$

$\mathcal{L} = [\hat{a}, \hat{b}, \hat{c}]$

Choose a random particle,  $c$

**for**  $l$  *in*  $\mathcal{L}$  **do**

$\mathcal{Q} = []$

**for**  $i \rightarrow (0, N)$  **do**

$\vec{v} = \vec{r}_i - \vec{r}_c$

$\hat{v} = \vec{v}/|\vec{v}|$

$\theta = \cos^{-1}(\hat{v} \cdot l)$

**if**  $\theta \leq \mathcal{X}_a$  **then**

$\mathcal{Q} \leftarrow i$

**end if**

**end for**

dist = []

**for**  $j$  *in*  $\mathcal{Q}$  **do**

$d = \frac{|\vec{r}_j - \vec{r}_c|}{|\vec{r}_j - \vec{r}_c|}$

dist  $\leftarrow$  d

**end for**

$d_{min} = \min(\text{dist})$

Get the index of  $\mathcal{Q}$  for which  $d_{min} = \min(\text{dist})$

**end for**

---

Once the coordinates of all eight corner particles in the parallelepiped are known, the estimation of the lattice parameters ( $a_d, b_d, c_d, \alpha_d, \beta_d, \gamma_d$ ) for the parallelepiped are carried out. The lattice parameters consisting of the length of each vector and angles between two unit vectors, are estimated from the joining vectors between each of  $N_1, N_2$  and  $N_3$  particles with  $N_0$  particle as the identities of the corner particles of the parallelepiped are sealed. The possible basis vectors of the parallelepiped are obtained by using equation 1 and 2 for a particular unit cell.

$$\vec{\mathbf{a}}_d = \vec{r}_1 - \vec{r}_0 \ \& \ \vec{\mathbf{b}}_d = \vec{r}_2 - \vec{r}_0 \ \& \ \vec{\mathbf{c}}_d = \vec{r}_3 - \vec{r}_0 \quad (1)$$



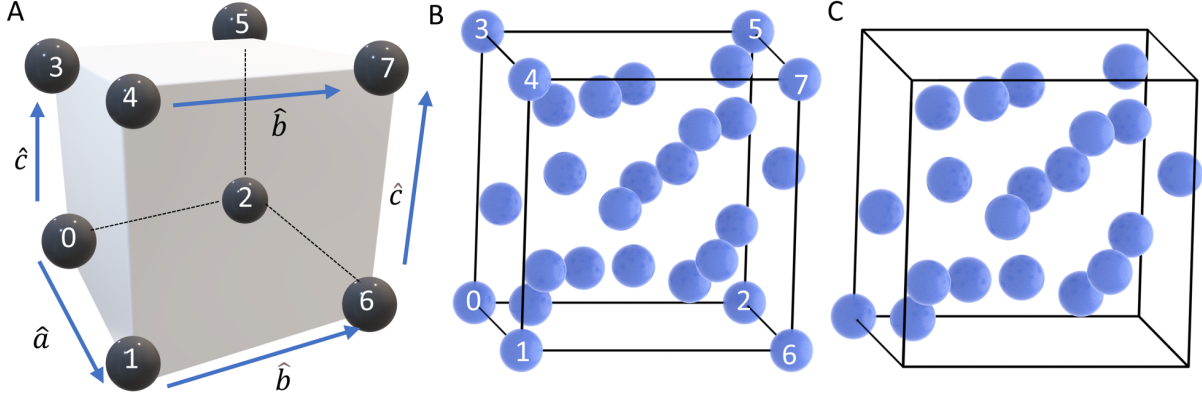


FIG. 11. (A) The corner particles of the unit cell translated along the three lattice vectors are shown in a cartoon diagram and (B) the unit cell of the considered system with all the particles including the corners is shown. The effective particle of an ideal  $\beta$ -Mn unit cell are evaluated and shown in (C).

$$\alpha_d = \cos^{-1}(\hat{\mathbf{b}}_d \cdot \hat{\mathbf{c}}_d) \ \& \ \beta_d = \cos^{-1}(\hat{\mathbf{a}}_d \cdot \hat{\mathbf{c}}_d) \ \& \ \gamma_d = \cos^{-1}(\hat{\mathbf{a}}_d \cdot \hat{\mathbf{b}}_d) \quad (2)$$

where  $\vec{r}_0$ ,  $\vec{r}_1$ ,  $\vec{r}_2$  and  $\vec{r}_3$  are the position vectors of  $N_0$ ,  $N_1$ ,  $N_2$  and  $N_3$  respectively. These vectors  $\vec{\mathbf{a}}_d$ ,  $\vec{\mathbf{b}}_d$ ,  $\vec{\mathbf{c}}_d$  are appended into another set  $\mathcal{P}_{all}$ . So, each element of the set  $\mathcal{P}_{all}$  corresponds to a possible triplet of basis vectors for the parallelepiped irrespective of satisfying any allowed Bravais unit cell or not, under the detected class.

## 2. All particle coordinates of the parallelepiped

The identification of the coordinates of all particles is needed to know the effective particles in the parallelepiped either it is a acceptable Bravais lattice or not. Using a triplet (may or may not be the basis vectors), we detect the eight corner particles of the parallelepiped. A convex-hull is formed with the coordinates of eight corner particles which act like an envelop. Considering the coordinates of all particles of the Bravais lattice, computationally we search the particles which lie inside the constructed convex hull using the *Delaunay* module of *Scipy*<sup>82</sup>. Following the method, we obtain all the particle coordinates staying inside the parallelepiped or on the face of the parallelepiped as shown in Fig. 11B. To handle the real data with noise, the hull is expanded isotropically by a volume factor ( $\mathcal{V}$ ), so that all the particles located at any sites other than the corners, can be found inside the convex hull. For example, if the initial or transformed Bravais system is face-centered lattice, the particles

exactly located on the faces of the parallelepiped (considered as the unit cell box) can not be obtained due to the noise present in the system. For that case, a little bit expansion of the convex hull is needed. For an ideal crystal structure,  $\mathcal{V}$  is set to 0. It is important to remember that for the successful execution of this step, we need to use the coordinates of the particles in the Bravais lattice only even if the initial system is a non-Bravais one.

### *3. Coordinates of effective particles in a parallelepiped*

After the identification of all particle coordinates in the parallelepiped formed by a particular triplet, we can check whether the parallelepiped represents a Bravais lattice or not, under the previously detected crystal class. The coordinates of the effective particles in the parallelepiped are needed to be detected to compare with the Bravais lattice.

Effective coordinates are related to one another by the crystallographic symmetry properties. In principle, all the particle coordinates in the unit cell can not be the effective particle coordinates. If the joining vector between any two particles of the parallelepiped,  $\vec{r}_{ij}$  does not coincide with any of the vector directions i.e.,  $\hat{\mathbf{a}}_d, \hat{\mathbf{b}}_d, \hat{\mathbf{c}}_d$  within the angle tolerance  $\mathcal{X}_a$  and the modulus of  $\vec{r}_{ij}$  i.e.,  $|\vec{r}_{ij}|$  sufficiently differs from any of the  $|\vec{\mathbf{a}}_d|, |\vec{\mathbf{b}}_d|, |\vec{\mathbf{c}}_d|$  respectively barring the distance tolerance  $\mathcal{X}_d$ , then the coordinate of the particle can not be generated from the other one by translating any of the vectors within the parallelepiped. So, two particles violating the condition are considered as equivalent particles and only one particle is recognized as effective particle instead of two. The algorithmic way of the determination of effective particles is described below.

---

**Require:** Coordinate of  $N_{uc}$  particles

$\mathcal{D} = []$

**for**  $i \rightarrow (0, N_{uc} - 1)$  **do**

**if**  $i$  not in  $\mathcal{D}$  **then**

**for**  $j \rightarrow ((i + 1), N_{uc})$  **do**

**if**  $j$  not in  $\mathcal{D}$  **then**

$$\vec{r}_{ij} = r_j - r_i$$

$$\hat{r}_{ij} = \frac{\vec{r}_{ij}}{|\vec{r}_{ij}|}$$

$$\Theta_1 = \cos^{-1}(\hat{r}_{ij} \cdot \hat{\mathbf{a}}), \Theta_2 = \cos^{-1}(\hat{r}_{ij} \cdot \hat{\mathbf{b}}), \Theta_3 = \cos^{-1}(\hat{r}_{ij} \cdot \hat{\mathbf{c}})$$

**if**  $\Theta_1 \leq \mathcal{X}_a$  or  $\Theta_2 \leq \mathcal{X}_a$  or  $\Theta_3 \leq \mathcal{X}_a$  **then**

**if**  $(|\vec{\mathbf{a}}| - \mathcal{X}_d) \leq |\vec{r}_{ij}| \leq (|\vec{\mathbf{a}}| + \mathcal{X}_d)$  or  $(|\vec{\mathbf{b}}| - \mathcal{X}_d) \leq |\vec{r}_{ij}| \leq (|\vec{\mathbf{b}}| + \mathcal{X}_d)$  or  $(|\vec{\mathbf{c}}| - \mathcal{X}_d) \leq |\vec{r}_{ij}| \leq (|\vec{\mathbf{c}}| + \mathcal{X}_d)$  **then**

$\mathcal{D} \leftarrow j$

**end if**

**end if**

**end if**

**end for**

**end if**

**end for**

$\mathcal{B} = []$

**for**  $i \rightarrow (0, N_{uc})$  **do**

**if**  $i$  not in  $\mathcal{D}$  **then**

$\mathcal{B} \leftarrow i$

**end if**

**end for**

---

Where  $N_{uc}$  is the total number of particles in the parallelepiped and  $\mathcal{B}$  is a list consisting the identities of the effective particle only. After the identification of the coordinates of the effective particles in a parallelepiped, we search for the unit cell of Bravais lattice under the detected crystal class that matches with the parallelepiped. A Bravais lattice is either a primitive cell or a “centered cell” with particles located at either on the face mid-points, base mid-points or center of the parallelepiped under a particular crystal class. Comparing

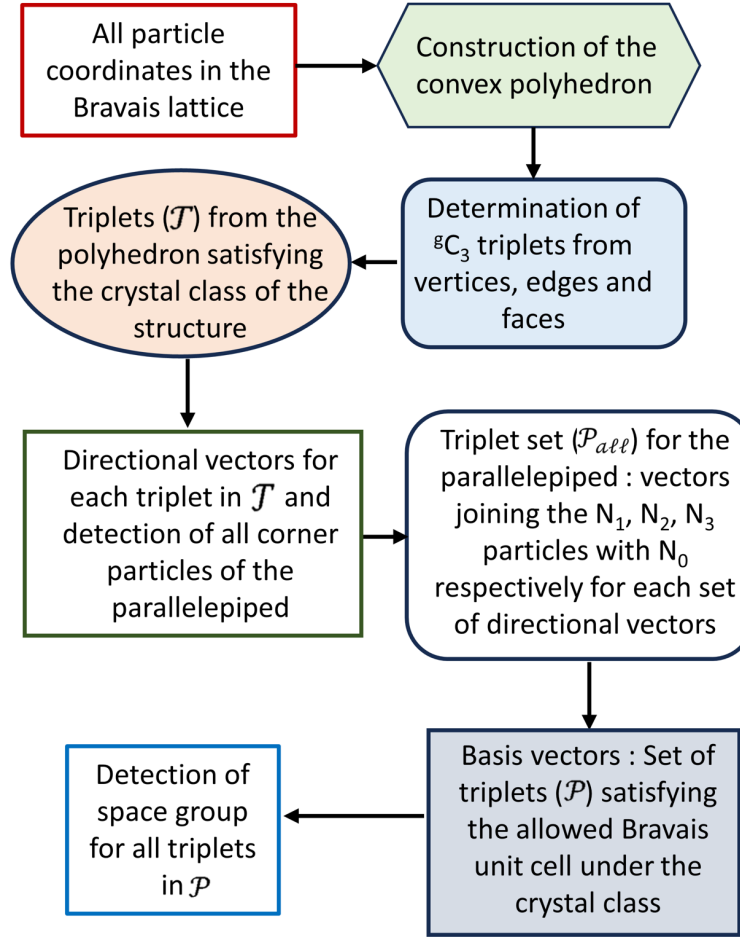


FIG. 12. A flowchart showing the space group detection for all basis vectors from the Bravais lattice

the coordinates of effective particles in the parallelepiped with all allowed Bravais lattices under the crystal class (as shown in Fig. 11A) barring a tolerance value in real system, the identification is carried out to make the decision about the chosen triplet from  $\mathcal{P}_{all}$  to be considered as basis vectors or not. Each possible triplet of the set  $\mathcal{P}_{all}$  is chosen and checked to be recognized as a valid choice of a permitted Bravais unit cell under the detected crystal class. In this way, all triplets satisfying the condition are identified and considered as a set  $\mathcal{P}$ , where total number of such triplets is  $n_p$ . As each of these triplets satisfies the requirement of an allowed Bravais unit cell, a triplet can be accepted as  $\vec{a}$ ,  $\vec{b}$ ,  $\vec{c}$ . A schematic diagram is presented in Fig. 12 describing the protocol of identification of the basis vectors for the structure. After identifying the allowed triplets for the basis vectors, the next step is to construct the unit cell of the initially considered structure which is discussed below.

#### D. Unit cell formation of the crystal structure

Each triplet of the set  $\mathcal{P}$  is considered that can span an allowed unit cell to generate the entire Bravais lattice. We detect only the corner particles of the Bravais unit cell for each triplet chosen from the set  $\mathcal{P}$  by searching the particles at the nearest distances followed by the construction of a convex hull as described earlier. Now all the particle coordinates of the initially considered system (a non-Bravais lattice if transformed) are taken into account and we find the coordinates of all particles in the unit cell by expanding the convex hull to handle the noise of the system, following the same protocol discussed in the above section. The unit cell for the considered crystal structure with all particle coordinates and basis vectors is formed leading to the determination of lattice parameters of the unit cell ( $a, b, c, \alpha, \beta, \gamma$ ). We also detect the coordinates of effective particles in the unit cell following the similar approach as discussed. Now all the necessary information of the unit cell is known for a particular choice of basis vectors and all the triplets of the set  $\mathcal{P}$  are allowed for the structure.

The choice of the lattice parameters of the determined unit cell for  $\beta$ -Mn crystal structure was unique and the values were  $a=6.3150024$ ,  $b=6.3150024$ ,  $c=6.3150024$ ,  $\alpha=90^\circ$ ,  $\beta=90^\circ$ ,  $\gamma=90^\circ$ , which exactly matched with the lattice parameters initially used to construct the unit cell<sup>9</sup>. The protocol confirmed that the unit cell of  $\beta$ -Mn crystal structure consisted of 20 effective particles and the coordinates were known.

#### E. Determination of space group of the crystal structure

As the final goal, we determine the space group of the considered crystal structure for a particular choice of basis vectors with the complete knowledge of the unit cell. For this, *Spglib* package is used to get all the crystallographic symmetry operations of the corresponding crystal structure and finally the space group. Computationally, we check for all the possible symmetry operations of the unit cell i.e. translation, rotation, reflection, screw axes and glide planes. This leads to the determination of the space group properly with a particular set of triplet for which the possible crystallographic symmetry operations are obtained and applied correctly. The three dimensional Cartesian coordinates of the effective particles are transformed into fractional coordinates and the lattice parameters along with

those fractional coordinates are used as inputs. All the possible crystallographic symmetry operations were checked computationally by the package within the tolerances (for ideal system, the tolerances are zero) and the space group of the crystal structure is obtained as outputs according to the standard nomenclature<sup>83</sup>. Space group detection is quite straightforward for an ideal crystal and it is complicated for a noisy crystal, as we need to tune two tolerance values, *symprec*, i.e. the distance tolerance in Cartesian coordinates and *angle\_tolerance* to determine the space group of the crystal structure as well as the all possible crystallographic symmetry operations. Unsuccessful determination of any symmetry operation can affect the space group leading to the determination of an incorrect one; so it is very sensitive on the tolerances. Corresponding crystallographic symmetry operations can also be obtained using the *get\_symmetry* module of the package specifying the lattice and basis information in proper format. The same space group is determined for all  $n_p$  choices of basis vectors of set  $\mathcal{P}$ . Multiple choices in the real-space do not affect the space group as a unique choice of fractional coordinates defining the symmetry of the crystal is obtained from any particular set of the effective particle coordinates and basis vectors. In general, the number of choices for basis vectors depends on the considered crystal structure. The algorithmic recipe not only provides the complete information of the unit cell and space group of the crystal structure but also the possible choices of the valid basis vectors are obtained. Considering the coordinates of the particles as the only inputs, the protocol provides the unit cell information and corresponding space group irrespective of any complex structure as shown by the schematic diagram in Fig. 13. The detail implementation is showcased step-by-step for the ideal  $\beta$ -Mn crystal structure in Fig. 14.

The space group of ideal  $\beta$ -Mn crystal appeared to be  $P4_132$  according to the international symbol as detected by the method where only one choice of the basis vectors ( $n_p = 1$ ) was observed. Each step of the detection of the unit cell of beta-Mn crystal structure is shown in Fig. 14. Further examples of simple and complex crystal structures will be discussed along with an example of a system directly obtained from simulation data. The results will mainly focus on the implementation of the scheme in different kinds of crystal structures as the validation purposes.

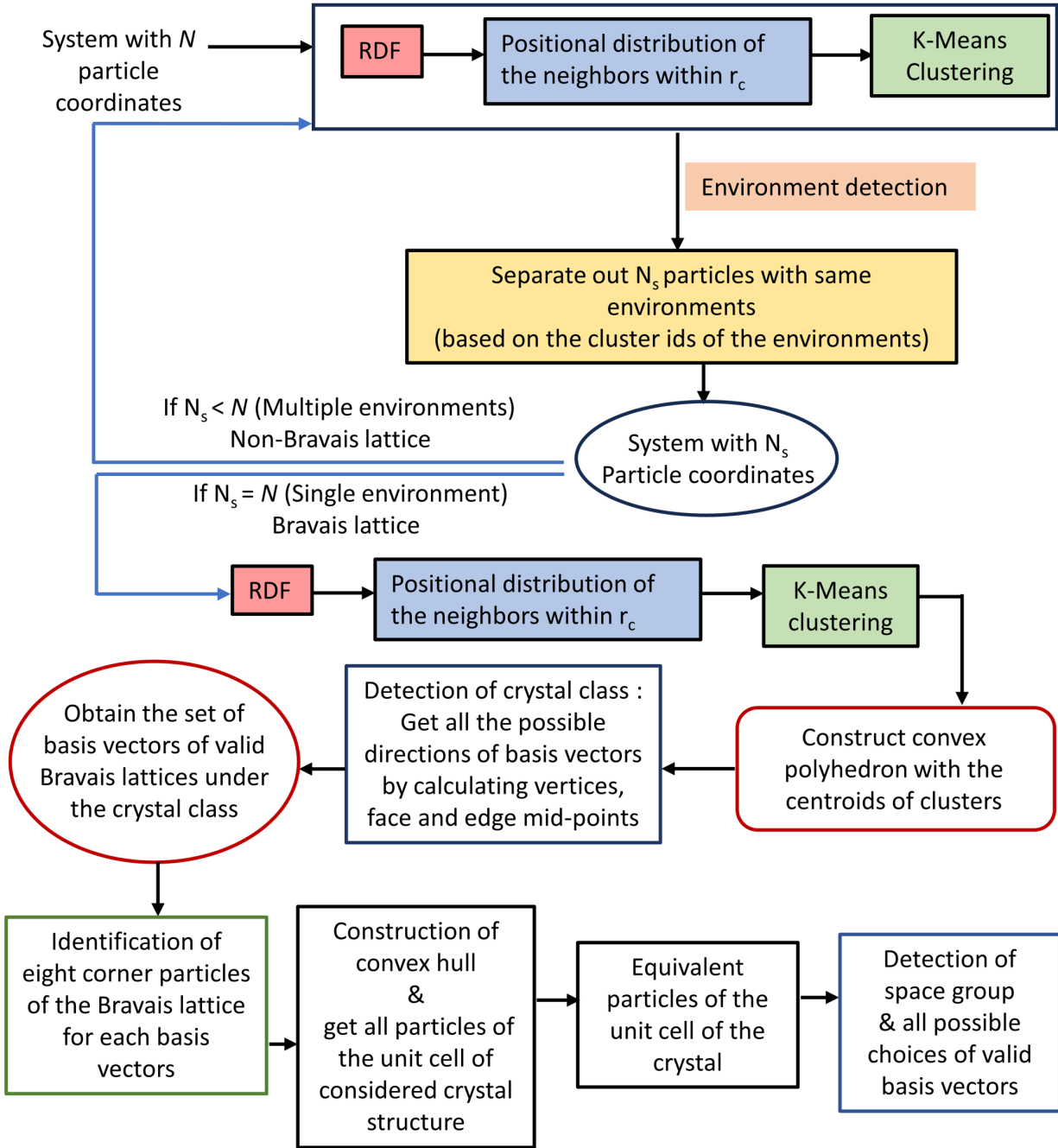


FIG. 13. The complete summary of the approach is illustrated in this figure.

## RESULTS AND DISCUSSION

In this research, the data of three synthetically prepared ideal crystalline systems are reported by replicating the corresponding unit cells (Crystallographic Information File, i.e., CIF files are available in Crystallographic Open Database (COD) system<sup>84</sup>) in three-

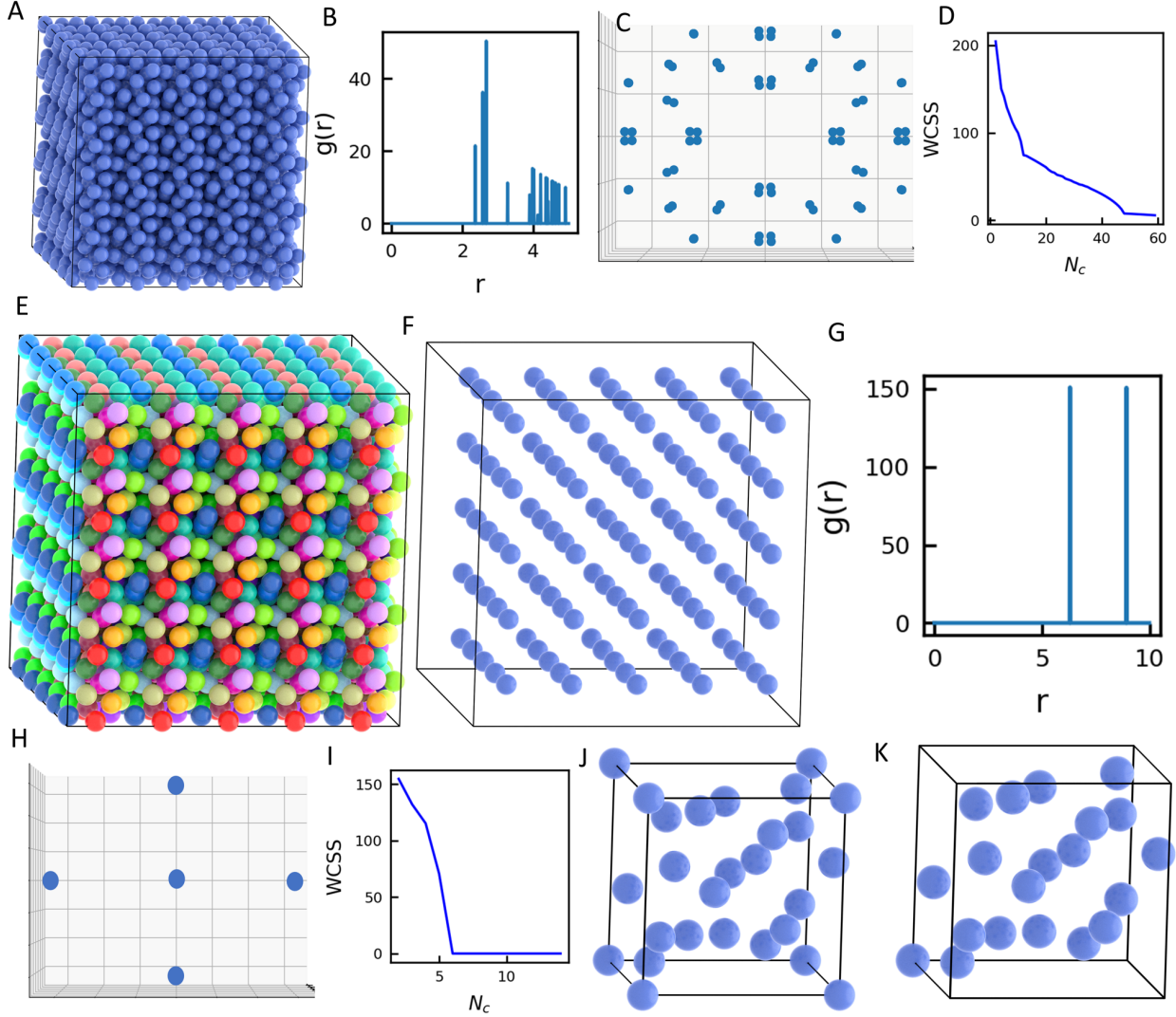


FIG. 14. (A) An ideal beta-Mn crystal structure is considered followed by the determination of radial distribution function (B), bond-orientational diagram (C) and the implementation of the *K-Means* clustering algorithm (D). As a part of the environment separation technique, the particles are colored based on the similar kind of environment and shown in (E). The particles sharing the similar kind of environment (particles with “blue” color only) are separated out as shown in (F). The radial distribution function (G), bond-orientational order diagram (H) and the *K-Means* algorithm (I) are implemented on the transformed Bravais lattice system. The unit cell of the system and effective particle are shown in (J) and (K) respectively.

dimensions where the lattice parameters and space group (as denoted by *International symbol*) are known. We applied the protocol and checked whether the same unit cell and space



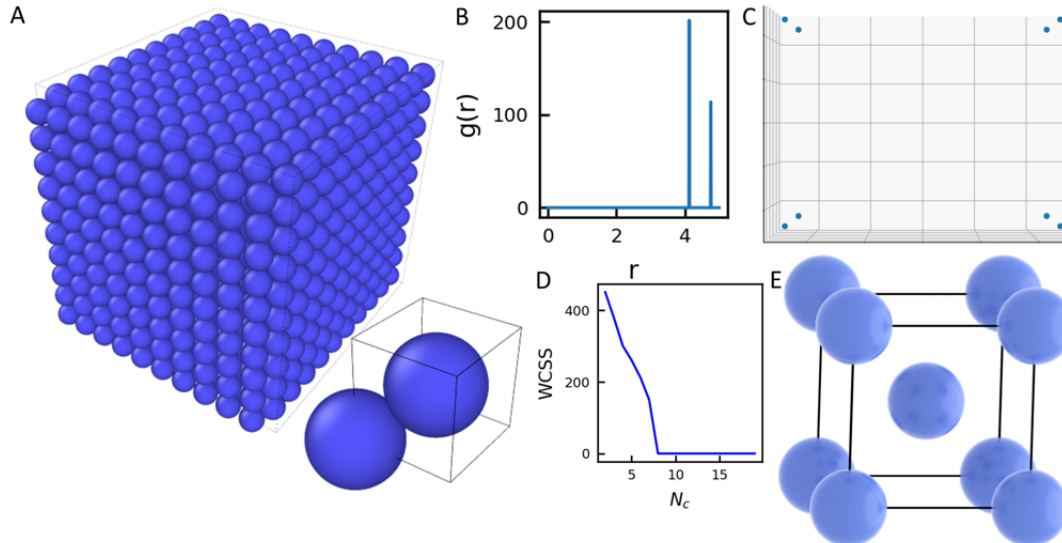


FIG. 15. (A) An ideal BCC crystal of Ba is shown along with the unit cell in the inset. RDF and the distribution of the first nearest-neighbors are shown in (B) and (C) respectively with  $r_c \sim 4.5$ . There are eight clusters as confirmed by elbow analysis of the *K-Means* clustering (D). The BCC unit cell contains total nine particles as shown in (E).

group can be obtained from the bulk crystal structure using the coordinates only. The detected unit cells of these systems along with all steps are shown below including the data of simulated cubic diamond crystal structure by varying the noise levels. Here, we demonstrate our approach using four crystal structures, (i) an ideal body-centred cubic (BCC) crystalline system with space group  $Im\bar{3}m$ , (ii) an ideal system of  $C_3O_6Sr$  monoclinic crystal with space group  $P12_1/C_1$ , (iii) a synthetically prepared Hexagonal-closed packed (HCP) structure with space group  $P6_3/mmc$  and (iv) the simulated cubic diamond crystal structures with space group  $Fd\bar{3}m$  and eight effective particles in the unit cell at different noises. The last example depicts the system with the different statistical noises as those comes out of computer simulations. The scheme is applied step by step on each system and the detected unit cells, space groups are shown as results.

Fig. 15A shows an ideal BCC crystal, manually generated from the unit cell of Barium (Ba) with lattice parameters  $a=4.758$ ,  $b=4.758$ ,  $c=4.758$ ,  $\alpha=90^\circ$ ,  $\beta=90^\circ$ ,  $\gamma=90^\circ$ <sup>85</sup> (inset of (A)), followed by a calculation of RDF of the system, showing crystal-like nature (Fig. 15B). The nearest neighbor distance ( $r_c$ ) is calculated from the first minima of the RDF which turned out to be  $\sim 4.5$  (exact nearest neighbor distance was 4.12). Further, considering

all pairwise distances, the positional distributions of the neighbors within  $r_c$  is shown in (Fig. 15C), formed eight particles (zero positional deviation for the ideal system) in three-dimensional space, as confirmed by the elbow analysis of *K-Means* clustering algorithm as in Fig. 15D. The environment separation was performed and it turned out that  $\sim 100\%$  particles had similar kind of environment confirming the system as a Bravais lattice already. For this example, the transformation from a non-Bravais lattice into a Bravais lattice was not required. The coordinates of the centroid of the clusters (here the coordinate of the particles in the BOO) were considered as the vertices of a convex polyhedron. After the decomposition of the convex polyhedron, the vertices forming the polyhedron's faces and edges were evaluated followed by the calculations of determining the coordinates of the six face mid-points and twelve edge mid-points. Total number of non-unit vectors ( $g$ ) calculated from the polyhedron was 26. Each triplet of  ${}^{26}C_3$  combinations was treated as a set of lattice vectors ( $\vec{\mathbf{a}}_d$ ,  $\vec{\mathbf{b}}_d$  and  $\vec{\mathbf{c}}_d$ ) and the lattice parameters,  $a$ ,  $b$ ,  $c$ ,  $\alpha$ ,  $\beta$  and  $\gamma$  were determined. Computationally we checked each set of lattice parameter to know the crystal class satisfied by the those. Cubic crystal class was satisfied by few triplets as the highest order of symmetry i.e., 48. The directions of basis vectors appeared to be unique satisfying the cubic class and  $\hat{\mathbf{a}} = [1, 0, 0]$ ,  $\hat{\mathbf{b}} = [0, 1, 0]$  and  $\hat{\mathbf{c}} = [0, 0, 1]$ . No other directions produced any valid Bravais lattices under the cubic class. Construction of the unit cell with the basis vectors followed the determination of actual lattice vectors,  $\vec{\mathbf{a}} = [4.758, 0, 0]$ ,  $\vec{\mathbf{b}} = [0, 4.758, 0]$  and  $\vec{\mathbf{c}} = [0, 0, 4.758]$  with lattice parameters 4.758, 4.758, 4.758,  $90^\circ$ ,  $90^\circ$ ,  $90^\circ$ . The BCC unit cell with eight particles at corners and one particle at the centre of the cubic box was obtained as shown in Fig. 15E. The two effective particles were obtained and the space group detection technique was applied with four particle basis and the space group turned out to be  $Im\bar{3}m$  considering  $symprec = 0.0$  and  $angle\_tolerance = 0^\circ$ .

Another ideal atomic crystal of  $C_3O_6Sr$  (space group -  $P_12_1/C_1$ ) with complex basis was prepared with lattice parameters,  $a = 7.966$ ,  $b = 9.205$ ,  $c = 7.319$ ,  $\alpha = 90^\circ$ ,  $\beta = 102.104^\circ$  and  $\gamma = 90^\circ$ <sup>86</sup>. Fig. 17A exhibits the synthetically prepared crystal structure by replicating the unit cell in the three dimensions, where the unit cell is shown in the inset of Fig. 17A. Only the coordinates of each kind of atoms were considered irrespective of their sizes or atom types and the configuration is shown in Fig. 17B. We intentionally loose all the information except the coordinates of all particles for the validation purpose. The RDF was calculated and the value of  $r_c$  was chosen as 1.2. The positional distribution of nearest neighbors within  $r_c$  is

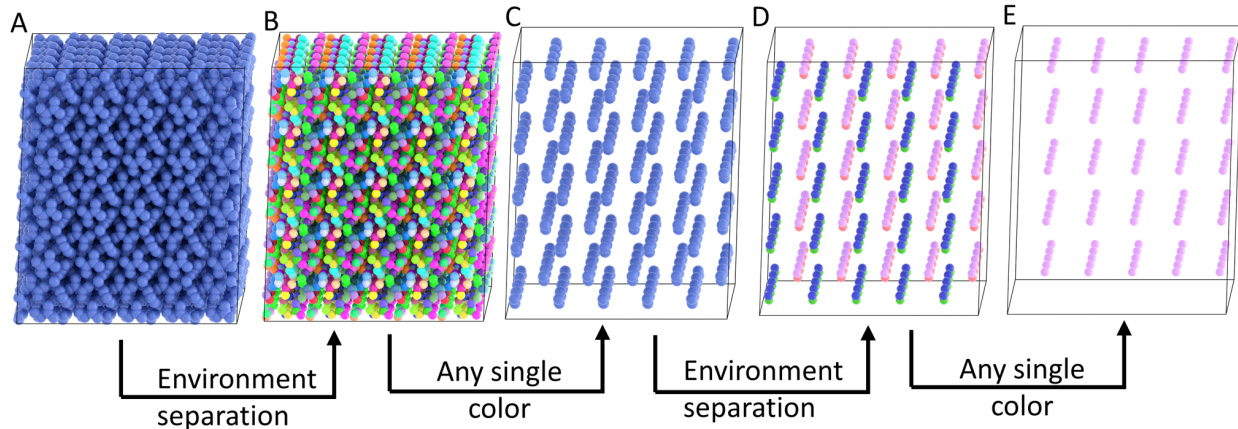


FIG. 16. Environment separation technique was carried out on the system of  $C_3O_6Sr$  crystal showing the transformation of the complex non-Bravais structure into a “simple cubic” Bravais lattice at two steps. The initial non-Bravais lattice is shown in (A). After categorizing based on the environments, the particles are shown in different colors, where the particles with any single color have the similar kind of environment (B). The configuration with only blue color was chosen as system (C) followed by the categorization of the particles based on the the environments as shown in (D). Then the transformation of the Bravais lattice successfully happened after separating out the particles with the “pink” color only from the system (D) as shown in (E).

shown in Fig. 17D. Only four clusters were detected as confirmed by the elbow analysis after the *K-Means* clustering (Fig. 17E) was done. The environment separation technique was carried out two times in the iterative way, until each particle had similar kind of positional environment in the transformed system, i.e. the non-Bravais lattice turned into a Bravais lattice. The configurations of the two steps are shown in Fig. 16, with the categorization of the particles based on the cluster ids in the corresponding BOOs. After the transformation, the system snapshot is shown in Fig. 17F. Hence the “pink” color of the particles in the Cubic Bravais lattice (shown in Fig. 16E) was changed into “blue” color (Fig. 17F) for the visualization purposes only, where the coordinates of the particles in the two systems shown at Figs. 16E, 17F were kept intact except for the color. The RDF was calculated further and shown in Fig. 17G and  $r_c$  was chosen as 9.99, confirming the distribution of the positions of the nearest neighbors in three-dimensional coordinate system as shown in Fig. 17G. Eight distinct clusters (for ideal system, only particles) were found (Fig. 17H), which is confirmed by the elbow analysis plot of *K-Means* clustering (Fig. 17I). Construction of the convex

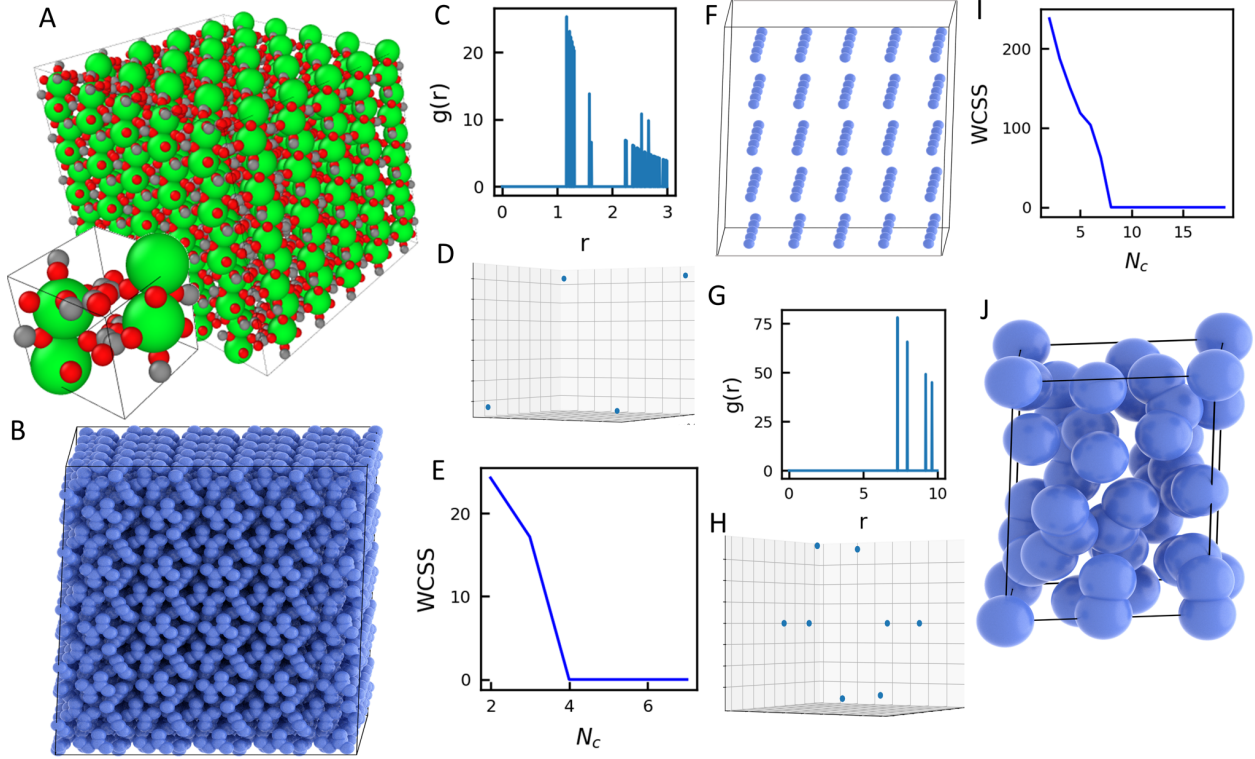


FIG. 17. (A) An ideal multi-component monoclinic crystal of  $C_3O_6Sr$  is shown along with the unit cell (inset). The effective coordinate of the particles irrespective of the size or particle types are shown in (B), followed by the corresponding RDF and distribution of first nearest-neighbor in (C) and (D) respectively. Number of clouds with zero positional deviation is four as confirmed by the elbow analysis of *K-Means* clustering (E). After environment separation for five times, using the particles sharing the same kind of environment, the system snapshot is shown in (F) RDF is calculated (G). Choosing  $r_c \sim 9.5$ , the positions of the local neighbors are illustrated in (H). There exists eight unique clusters according to (I) and the monoclinic unit cell is shown in (J).

polyhedron provided the directions of fifteen possible vectors, but all those triplets did not replicate the valid unit cell under Monoclinic crystal class. We separated out the basis vectors corresponding to the primitive Monoclinic unit cell with one effective particle and there were eight unique choices. A single triplet from the set of eight choices was considered and the unit cell of the crystal structure was detected. One of the valid choices of basis vectors was  $\vec{a} = [-2.448, 0, -7.157]$ ,  $\vec{b} = [-4.750, 0, 3.578]$  and  $\vec{c} = [0.0, -9.205, 0.0]$  and the lattice parameters were  $7.966, 9.205, 7.319, 90^\circ, 102.104^\circ, 90^\circ$  along with other seven possible choices. For the validation purpose, the unit cell of the crystal structure was generated by

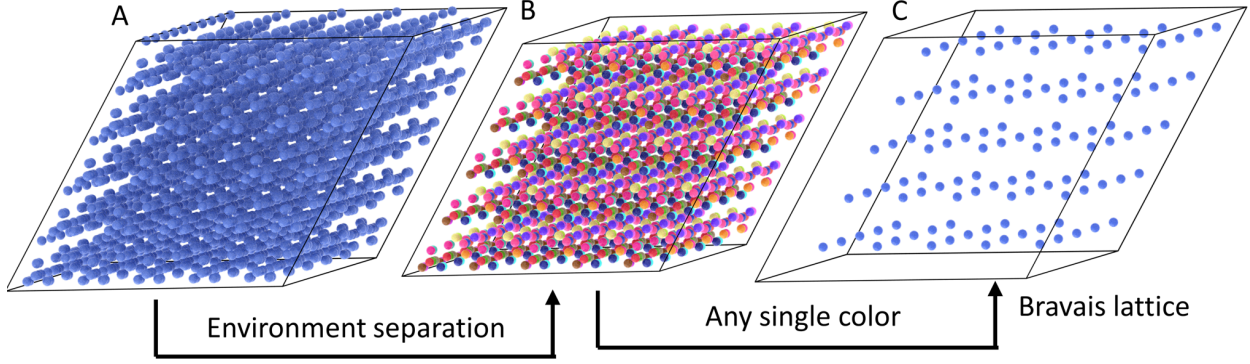


FIG. 18. Transformation of a complex Hexagonal-closed packed (HCP) structure into a Bravais lattice is shown using the “environment separation” technique. (A) The particle coordinates in a synthetically prepared ideal HCP crystal structure are shown. After categorizing the particles based on the environments, the configuration is shown (B), where particles with same color have similar kind of environment in the configuration. (C) Finally the particles with any color (here “blue” color) are chosen and the system satisfies the criteria of a Bravais lattice.

translating along the directions of that basis vectors. After obtaining eight corner particles of the Monoclinic cell, the convex hull was constructed followed by the detection of the coordinates of all particles in the unit cell for the initial non-Bravais lattice system. As this was an ideal structure without noise, the expansion parameter of the convex hull  $\mathcal{V}$  was set to zero. A randomly chosen unit cell is shown in Fig.17J, which confirms the lattice parameters to be exactly same as our initial consideration where all other choices of different lattice parameters were present with different basis vectors. The unit cell fails to provide any atomic information of the basis upon the execution of the algorithm as we have used the coordinates only by discarding all other details. The space group appeared to be  $P_12_1/C_1$  for each of the eight choices, which validates the success of the methodology towards the determination of unit cell of the crystal structure in the real-space.

The next example is the detection of the unit cell and a space group of a synthetically prepared ideal Hexagonal-closed packed (HCP) structure with lattice parameters 5.947, 5.947, 8.375,  $90^\circ$ ,  $90^\circ$ ,  $120^\circ$  and space group  $P6_3/mmc$ , having 22 effective particles in the unit cell. Our aim was to get back the exact lattice parameters and the space group following the defined approach, as used to construct the HCP structure. The coordinates of the particles were considered from the HCP crystal structure of  $K_2SO_4$  by losing all other information

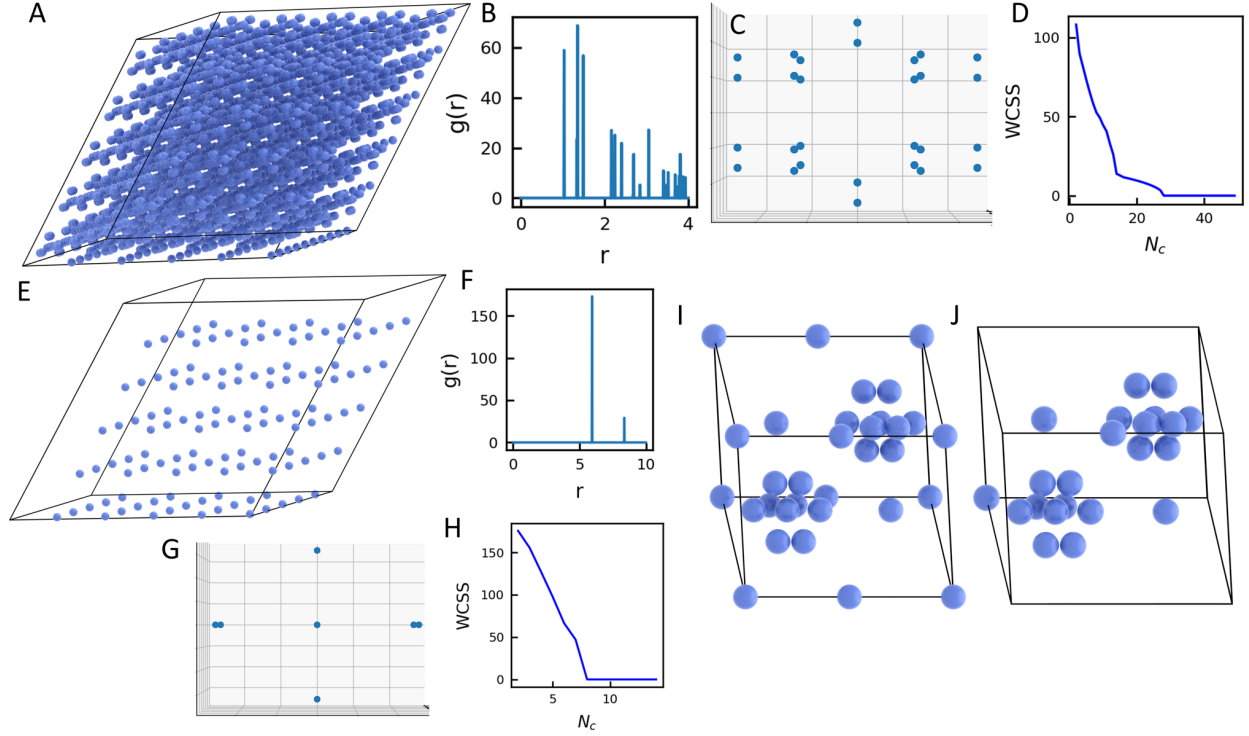


FIG. 19. The steps are shown for a synthetically prepared HCP crystal structure. (A) The coordinates of the particles are shown followed by the calculation of RDF (B), BOO (C) and elbow analysis after *K-Means* clustering (D). After separating the particles with similar environment for two times as shown in the Fig. 18, the transformed Bravais system is shown in (E). Considering the Bravais lattice, again the RDF (F), BOO (G) and the elbow analysis (H) are calculated. All particles in the unit cell and effective particles of the HCP structure are shown in (I) and (J) respectively.

intentionally expect the coordinates of the atoms, already reported in the literature<sup>87</sup>. The steps to separate the particles with similar kind of environment are illustrated in Fig. 18. The coordinates of the particles of a HCP structure are shown in Fig. 18A. As the first step of the layout, we checked whether the considered system was a Bravais lattice or not. To check this, the “environment separation” technique was carried out and the particles were categorized based on the unique environments. The configuration shown in Fig. 18B suggested that the considered system was non-Bravais in nature due to the existence of multiple kind of environments, as the particles with multiple colors existed. As the part of the “environment separation” technique, the particles with any single color (for this example, “blue”

color) were chosen (Fig. 18C) and considered further to check that whether the extracted system (Fig. 18C) was Bravais or not. The configuration shown in Fig. 18C turned out to be a hexagonal Bravais lattice, satisfying all the particles with similar kind of environment. For this structure the transformation of a non-Bravais lattice into a Bravais lattice occurred in a single iterations. The other steps of the scheme are described in Fig. 19. The coordinates of the particles in the HCP structure were considered as the initial system followed by a calculation of the RDF (Fig. 19B) where  $r_c \sim 2.0$ . The three dimensional distributions of the local neighbors within the distance  $r_c$  included 28 clusters (here only the points due to the ideal structure) as confirmed by the elbow analysis after the *K-Means* clustering was done (Fig. 19D). After separation of the environments (as described in Fig. 18), the hexagonal Bravais lattice was obtained and shown in Fig. 19E. The two configurations in Fig. 18E and Fig. 19E are exactly same. Considering the Bravais lattice, the RDF was calculated again with  $r_c$  chosen at 6.0 (Fig. 19F). The positional distribution of the local neighbors of all particles within the distance (Fig. 19G) suggests the existence of eight clusters (here only points) as assured by the elbow analysis shown in Fig. 19H. After the construction of convex polyhedron, all possible directions of the vectors,  $\hat{\mathbf{a}}_d, \hat{\mathbf{b}}_d, \hat{\mathbf{c}}_d$  were found. The valid choice of the directions of the primitive vectors appeared to be unique for this primitive Hexagonal Bravais lattice. Considering a reference particle from the Bravais lattice, the other seven corner particles were found by translating along each of the three primitive vector directions based on the minimum distances. Here both the tolerances,  $\mathcal{X}_d$  and  $\mathcal{X}_a$  were set to zero as there was no noise in the system. The lattice parameters calculated using the protocol were 5.947, 5.947, 8.375, 90°, 90°, 120°, satisfying the Hexagonal crystal class. The exact lattice vectors for the system were  $\vec{\mathbf{a}} = [5.947, 0, 0]$ ,  $\vec{\mathbf{b}} = [2.973, 5.15, 0]$  and  $\vec{\mathbf{c}} = [0, 0, 8.375]$ . After the formation of the convex hull with eight corner particles, all other particles except the eight corner ones, participating in the unit cell were found and shown in  $\mathcal{X}_d$ I. The coordinates of the effective particles were searched (shown in  $\mathcal{X}_d$ J) in order to calculate the space group and the space group turned out to be  $P6_3/mmc$ . For this example also, the defined methodology performed well and detected the unit cell as well as the space group of the crystal structure accurately.

The last example corresponds to the cubic diamond structure with complex basis, coming out of simulation<sup>38,40,65,70,88,89</sup>. The configuration is shown in Fig. 20A along with the RDF, BOO and elbow analysis after the *K-Means* clustering as shown in Fig. 20B,C,D. For this

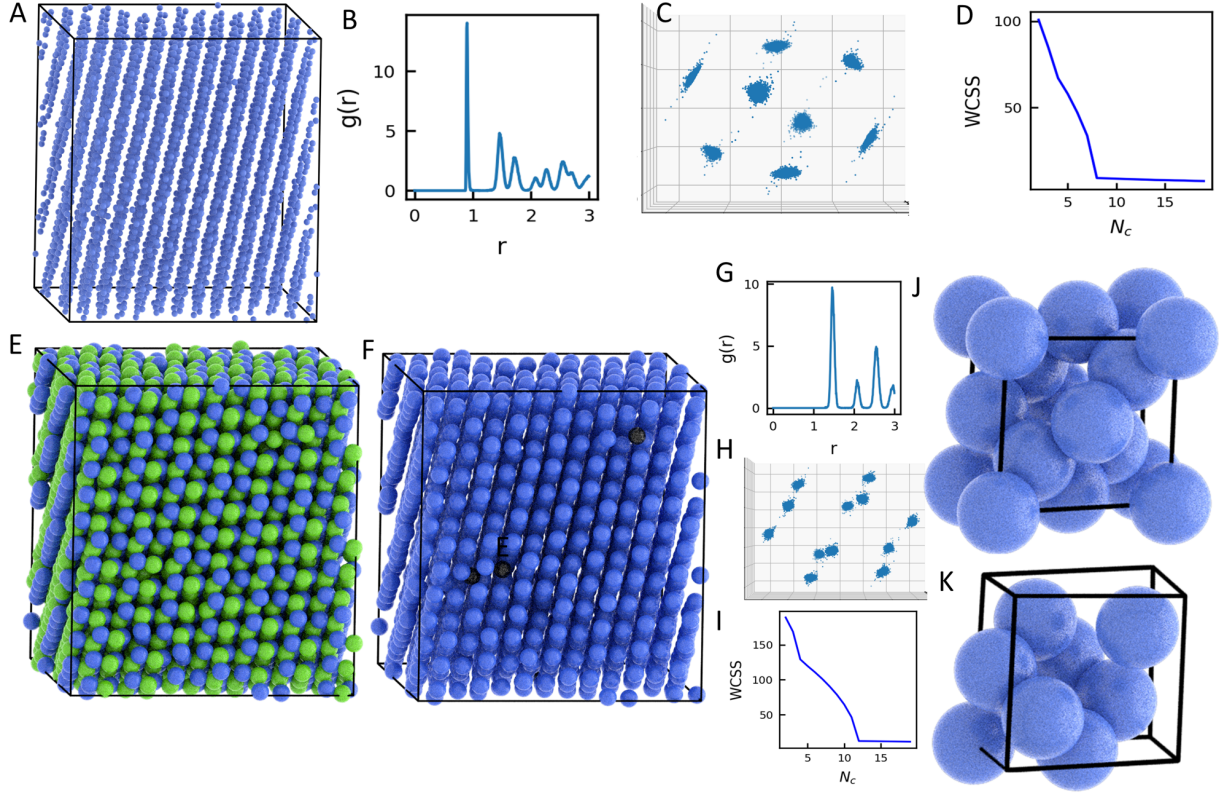


FIG. 20. (A) A system of cubic diamond crystal structure (complex basis) is shown along with the determination of corresponding RDF (B), the positional distribution of all neighbors in the system (BOO) (C) and elbow analysis of the *K-Means* clustering (D). After environment separation, the particles are shown in different colors in (E) based on the environments showing majority of the particles to have two distinct colors, “blue” and “green”. The rest of the colors are in very less in number; those can be treated as noise. The coordinates of the particles with only one color (“blue”) was separated out and considered as the system as shown in (F) followed by the determination of the RDF (G), BOO (H) and elbow analysis after the *K-Means* clustering (I). Finally the unit cell of the cubic diamond structure and eight effective particles in the unit cell are shown in (J) and (K) respectively.

structure,  $r_c$  was chosen as 1.1 as the first minima of the RDF distribution. Unlike the previous ideal systems, because of the statistical noise, total eight clusters of particles with significant positional deviations were observed followed by a confirmation of eight clusters by the elbow analysis of *K-Means* clustering. The environment separation technique was carried out on the system to categorize the particles based on the environments around themselves.



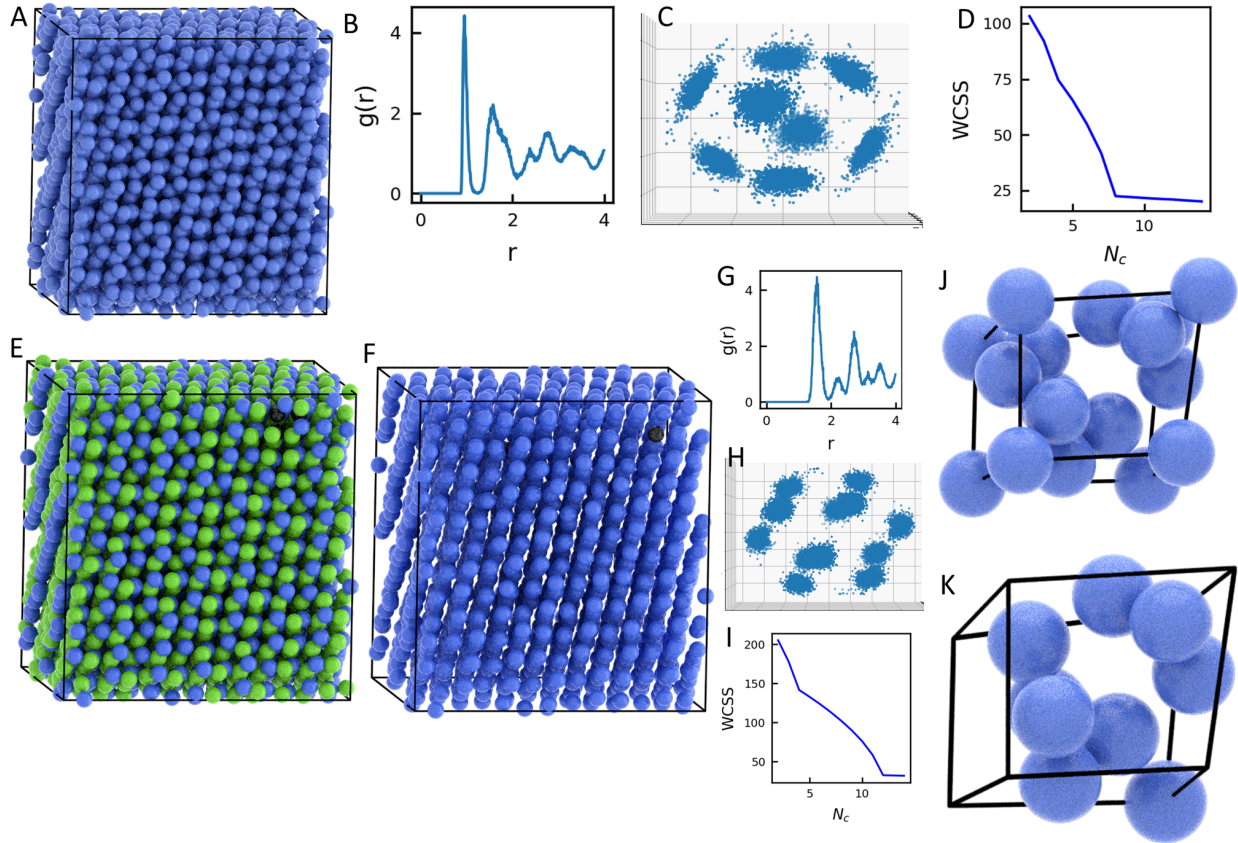


FIG. 21. All the steps are showcased for a system of the cubic diamond crystal with higher noise level than the system shown in Fig. 20. The numbers of the subfigures follow the same as defined in Fig. 20.

The configuration shown in Fig. 20E showed the majority of the particles in mainly two colors, “blue” and “green”, where the rest of the colors could be treated as noise due to the very less occurrence of such particles. By checking the environment,  $\sim 48.73\%$  particles of the initial considered system appeared to possess the similar kind of environment and was shown in Fig. 20E. As the next step, the particles having similar kind of environment, i.e., the particles with similar color (let’s say, “blue” color) were separated out and the coordinates of those particles were treated as the system of consideration for performing the next few steps. The particles in the “black” color as shown in the configuration (Fig. 20F) can be considered as noise. For this case the environment was separated within one iteration resulting  $\sim 93\%$  particles in the updated system had the similar kind of environment, satisfying the criteria of the Bravais lattice in the presence of the noise. Unlike te previous systems with the Simple Cubic (SC) Bravais lattice, here the transformed Bravais unit cell appeared to be

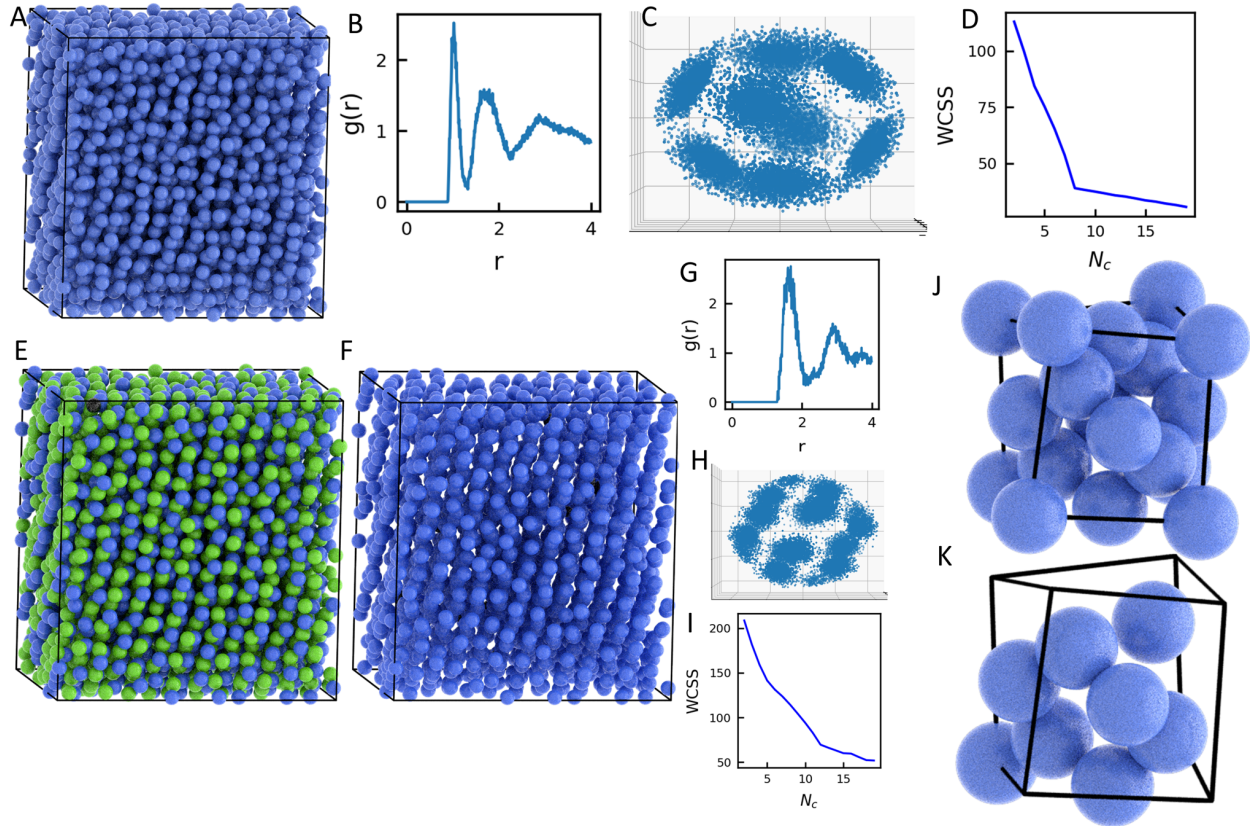


FIG. 22. All the steps are shown for a much higher noisy system of the cubic diamond crystal than the system shown in Fig. 20. The numbers of the subfigures follow the same as defined in Fig. 20.

FCC in nature. The RDF, BOO and *K-Means* clustering were analysed for the Bravais lattice exhibiting standard signature of FCC crystal Fig. 20G,H,I; where  $r_c$  was set at  $\sim 1.75$ . In the transformed FCC crystal, twelve distinct clusters were observed as assured by the elbow analysis of *K-Means* clustering. Consideration of the centroid of the twelve clusters as the vertices of a convex polyhedron, the coordinates of 14 face mid-points and 24 edge mid-points provided a total of 50 non-unit directions as designed in the protocol. All possible combinations of  ${}^{50}C_3$  were calculated as we got a set of possible triplets. We checked each triplet to satisfy the possible crystal classes within the tolerance values. The crystal class appeared to be cubic as it turned out to be of the highest order satisfied by a particular triplet. The choice of the primitive vectors appeared to be unique for simple cubic unit cell which were  $\vec{\mathbf{a}} = [-0.395, 0.212, -0.940]$ ,  $\vec{\mathbf{b}} = [-0.534, 0.811, 0.383]$  and  $\vec{\mathbf{c}} = [-0.791, -0.646, 0.216]$  which did not commensurate with the simulation frame. Choosing one random particle from the system and associating it with a lattice site, we translated

along the directions of primitive lattice vectors and got all the corner particles of the unit cell. After the construction of the convex hull using eight corner particles of the transformed Bravais lattice, the hull was expanded a little bit to handle the noise of the system, i.e.  $\mathcal{V} = 0.1$  times multiple of the total volume of the hull. All the particles in a randomly chosen cubic diamond unit cell are shown in Fig. 20J. Constructing the unit cell, the actual lattice vectors were evaluated followed by the determination of the lattice parameters;  $a= 2.101$ ,  $b=2.107$ ,  $c=2.16$ ,  $\alpha = 89.87^\circ$ ,  $\beta=89.30^\circ$  and  $\gamma=88.88^\circ$ . The effective particles in the unit cell are shown in Fig. 20K and the space group was also checked for the unit cell of the cubic diamond structure, which appeared to be  $Fd\bar{3}m$  with the consideration of two tolerances;  $symprec = 0.1$  and  $angle\_tolerance = 6^\circ$ .

The same strategy was applied on the cubic diamond crystal structures considering two different level of noises, to test the validity of the method. The systems shown in the Figs. 21, 22 correspond to the cubic diamond structure simulated at two lower packing fractions than the previous one (shown in Fig, 20). Bond-order diagrams (Fig. 20C, 21C, 22C) could be used as the standard visual descriptor of statistical noise, which suggest that the system shown in Fig. 22 is more noisy than the other two. The Figs. 21, 22 suggest the robustness of the methodology satisfying the same type of unit cell with eight effective particles and same fractional coordinates in the reference frame of the corresponding unit cell of the cubic diamond structure. Only the unit cells got distorted little bit depending on the noise present in the crystal structures. Except the fact, all the steps exhibited the same qualitative behavior as showcased in Figs. 21, 22. The positional deviation of the points in the distribution of the local neighbors (Fig. 21C and 22C) are much higher as compared to the same of Fig. 20C resulting the same transformed FCC crystals each time. Only the distance and angle tolerances used to handle the noisy crystal structures were little bit higher, which completely made sense. The tolerances were  $\mathcal{X}_d = 0.15$ ,  $\mathcal{X}_a = 10^\circ$  and  $\mathcal{X}_d = 0.2$ ,  $\mathcal{X}_a = 15^\circ$  for the noisy crystals shown in Figs. 21, 22 respectively. The same space group  $Fd\bar{3}m$  appeared for each of the cases indicating the robustness of the approach.

### III. CONCLUSIONS

We developed a direct approach to detect the unit cell and space group of the crystal structure based on the real-space analysis. Despite the coordinates of the particles, the anal-

yses of RDF and BOO lack the precise information of the crystal structure. The prescribed route involves these steps which directly depend on the particle coordinates in the real space. We also use the positional distribution of the local neighbors to identify the directions of lattice vectors which is the most important and challenging step in this route. In order to tackle the problem, one fundamental step is to find out the crystal class among seven classes in three dimensions after decomposing a complex structure into a simple Bravais lattice. We develop a robust computational way based on the difference between the Bravais and non-Bravais lattice allowing the transformation of any complex non-Bravais crystal structure into one of the fourteen Bravais lattices in the three dimensions. We use the idea of effective particles depending on the distributions of the neighbors and the transformation of a complex crystal into a simple Bravais lattice allow us to detect the directions of lattice vectors in a much simpler way. Based on the observations we note that each direction of the lattice vectors intersect any of the vertices, face mid-points or edge mid-points of the convex polyhedron constructed from the BOO. The computational approach using the clustering method is used to deal with the noise present in the system. The identification of the primitive lattice vector directions from the simulated system is very crucial where the primitive lattice vectors do not commensurate with the simulation frame. This approach makes our goal more achievable in the context of the detection of the unit cell as the directions of the broken symmetries were identified. It is quite straightforward that for any structures with primitive unit cell, the directions of the primitive lattice vectors pass through any of the vertices of the constructed polyhedron. Upon the detection of the lattice vectors and coordinates of the effective particles all the crystallographic symmetry operations of the corresponding unit cell were obtained. Successful execution of the recipe determines the unit cell and space group of the crystal structure, which is reported in this article for the ideal systems and the simulated systems with different noise levels.

The rotational invariance property of the crystal structure, defined by Steinhardt *et al.* is widely used as a descriptors for the identification of FCC, BCC, HCP structures<sup>48</sup>, while Ackland-Jones order parameter also distinguishes the local environment of FCC, BCC and HCP<sup>90</sup>. These order parameters are also useful to distinguish the solid or liquid like particles. The usages are limited to a few specific crystal structures and lack the general approach to detect any crystal structures. The reported scheme can not be treated as a direct extension or one to one correspondence with either of former two approaches, commonly used

in the context of crystal structures detection. The polyhedral template matching method was reported to identify the local environment of a few crystal structures but this method does not work for any crystal structures specially for the structures with crystal classes of lower symmetries such as orthorhombic, monoclinic, triclinic due to the variation of the distributions of the local neighbors<sup>80</sup>. Unlike the blueprint discussed in this article, the former approaches were not capable to provide the complete information of the unit cell along with the space group, in the presence of translational broken symmetry state satisfying the global rotational invariance. We did not incorporate the concept of “Wyckoff positions” in the strategy, which is one of the most common attributes used to identify the crystal structures<sup>1,7</sup>. On the other hand, in the modern machine learning based approach, a lot of reported structures are required as footprints for purely training purposes with a well defined and general descriptor. Our direct approach promises to detect any single crystal structures including the structure with complex basis and takes minimal time to detect the crystal structure accurately.

As the limitations of the discussed policy, this can not be used to study the process of crystal nucleation which requires a major modifications to the approach. This particular approach needs the assurance of the structure to have the complete translationally broken symmetry state in three dimensions as it does not check whether the considered structure is a crystal or not. Again this will not be useful to study the poly-crystalline structure; the modifications or extensions are kept for further studies. The detection of space group for the chiral crystal structure may fail or yields incorrect result due to the inappropriate implementation of the “environment separation” protocol which requires to be modified according to the chirality<sup>91</sup>. If the simulated crystal structure is too much noisy, one will definitely find difficulties to detect the unit cell of the crystal as the method fails to find the exact number of the clusters formed by the neighbors. Despite the dependency of the difficulty level on the noise present in the system, the methodology is robust, exact and converges. Only three dimensional crystal structures can be handled following the protocol; the implementation in any other dimensions are kept for further investigations. The method depends on some tolerance values, which strictly depend on the noise present in the crystal structures. Despite a few restrictions in the context of the application of computational layout, this promising approach is very useful to detect the crystal structures from real-space data in the field of condensed matter physics, applied physics or material sciences.

## ACKNOWLEDGMENTS

We acknowledge financial support from DST-INSPIRE Fellowship (IVR No. 201800024677) provided to SK. AD thanks DST-SERB Ramanujan Fellowship (SB/S2/RJN-129/2016) and IACS start-up grant. KC thanks IACS for financial support. Computational resources were provided by IACS HPC cluster and partial use of equipment procured under SERB CORE Grant No. CRG/2019/006418.

## AUTHOR DECLARATIONS

### Conflict of Interest

The authors have no conflicts to disclose.

### Author Contributions

SK and AD designed the research. SK and KC executed the idea computationally and implemented on multiple systems. SK and AD wrote the paper.

## DATA AVAILABILITY

The data that support the computational approach of this method are available within the article.

## REFERENCES

- <sup>1</sup>C. Kittel, *Introduction to Solid State Physics*, 8th ed. (Wiley, 2005).
- <sup>2</sup>V. W. Friedrich, P. Knippiig, M. A. L. V. von Sommerfeld, and von M Laue EinleituDg Barklas, “Interferenz-erscheinungen bei röntgenstrahlen,” *Theoretischer Teil* , 303–333 (1912).
- <sup>3</sup>“On the direct or indirect nature of the ionization by x-rays,” *The London, Edinburgh, and Dublin Philosophical Magazine and Journal of Science* **23**, 647–650 (1912).
- <sup>4</sup>W. H. Bragg, “The structure of the diamond,” *Nature* **91**, 557 (1913).

- <sup>5</sup>C. Davisson and L. H. Ghrmer, “Diffraction of electrons by a crystal of nickel,” *Physical Review* **30**, 705–737 (1927).
- <sup>6</sup>C. Giacovazzo, *Fundamentals of crystallography* (International Union of Crystallography, 1992) p. 654.
- <sup>7</sup>W. Massa, *Crystal Structure Determination* (Springer Berlin Heidelberg, 2004).
- <sup>8</sup>B. T. Willis, “Some achievements in neutron crystallography,” *Acta Crystallographica Section A: Foundations of Crystallography* **54**, 914–921 (1998).
- <sup>9</sup>W. Xie, S. Thimmaiah, J. Lamsal, J. Liu, T. W. Heitmann, D. Quirinale, A. I. Goldman, V. Pecharsky, and G. J. Miller, “beta-mn-type  $\text{Co}_{0.8}\text{Zn}_{1.2-x}$  as a defect cubic laves phase: Site preferences, magnetism, and electronic structure,” *Inorganic Chemistry* **52**, 9399–9408 (2013).
- <sup>10</sup>V. R. Dubach and A. Guskov, “The resolution in x-ray crystallography and single-particle cryogenic electron microscopy,” *Crystals* **10**, 1–13 (2020).
- <sup>11</sup>K. Amann-Winkel, M. C. Bellissent-Funel, L. E. Bove, T. Loerting, A. Nilsson, A. Paciaroni, D. Schlesinger, and L. Skinner, “X-ray and neutron scattering of water,” *Chemical Reviews* **116**, 7570–7589 (2016).
- <sup>12</sup>B. Deng and L. D. Marks, “Theoretical structure factors for selected oxides and their effects in high-resolution electron-microscope (hrem) images,” *Acta Crystallographica Section A: Foundations of Crystallography* **62**, 208–216 (2006).
- <sup>13</sup>A. Saha, S. S. Nia, and J. A. Rodríguez, “Electron diffraction of 3d molecular crystals,” *Chemical Reviews* **122**, 13883–13914 (2022).
- <sup>14</sup>C. Computational, “The ccp4 suite: Programs for protein crystallography,” (1994).
- <sup>15</sup>G. M. Sheldrick, “Crystal structure refinement with shelxl,” *Acta Crystallographica Section C: Structural Chemistry* **71**, 3–8 (2015).
- <sup>16</sup>O. V. Dolomanov, L. J. Bourhis, R. J. Gildea, J. A. Howard, and H. Puschmann, “Olex2: A complete structure solution, refinement and analysis program,” *Journal of Applied Crystallography* **42**, 339–341 (2009).
- <sup>17</sup>M. B. Zanjani, I. C. Jenkins, J. C. Crocker, and T. Sinno, “Colloidal cluster assembly into ordered superstructures via engineered directional binding,” *ACS Nano* **10**, 11280–11289 (2016).
- <sup>18</sup>T. Li, A. J. Senesi, and B. Lee, “Small angle x-ray scattering for nanoparticle research,” (2016).

- <sup>19</sup>J. Park, H. Zheng, W. C. Lee, P. L. Geissler, E. Rabani, and A. P. Alivisatos, “Direct observation of nanoparticle superlattice formation by using liquid cell transmission electron microscopy,” *ACS Nano* **6**, 2078–2085 (2012).
- <sup>20</sup>D. A. Keen and A. L. Goodwin, “The crystallography of correlated disorder,” *Nature* **521**, 303–309 (2015).
- <sup>21</sup>Y. J. Lu, J. Kim, H. Y. Chen, C. Wu, N. Dabidian, C. E. Sanders, C. Y. Wang, M. Y. Lu, B. H. Li, X. Qiu, W. H. Chang, L. J. Chen, G. Shvets, C. K. Shih, and S. Gwo, “Plasmonic nanolaser using epitaxially grown silver film,” *Science* **337**, 450–453 (2012).
- <sup>22</sup>R. L. Harlow, “Troublesome crystal structures: Prevention, detection, and resolution,” *J. Res. Natl. Inst. Stand. Technol* **101**.
- <sup>23</sup>M. Siczek, M. Zawadzki, M. Siczek, A. Chłopaś-Konowalek, and P. Szpot, “Etazene (n,n-diethyl-2-[(4-ethoxyphenyl)methyl]-1H-benzimidazol-1-yl)-ethan-1-amine (dihydrochloride)): a novel benzimidazole opioid nps identified in seized material: crystal structure and spectroscopic characterization,” *Forensic Toxicology* **39**, 146–155 (2021).
- <sup>24</sup>A. Dawson, D. R. Allan, S. Parsons, and M. Ruf, “Use of a ccd diffractometer in crystal structure determinations at high pressure,” *Journal of Applied Crystallography* **37**, 410–416 (2004).
- <sup>25</sup>X. H. Zhu, Z. R. Wei, Y. R. Jin, and A. P. Xiang, “Growth and characterization of a pbi2 single crystal used for gamma ray detectors,” *Crystal Research and Technology* **42**, 456–459 (2007).
- <sup>26</sup>J. V. D. Streek and M. A. Neumann, “Validation of molecular crystal structures from powder diffraction data with dispersion-corrected density functional theory (dft-d),” *Acta Crystallographica Section B: Structural Science, Crystal Engineering and Materials* **70**, 1020–1032 (2014).
- <sup>27</sup>D. H. Son, S. M. Hughes, Y. Yin, and A. P. Alivisatos, “Cation exchange reactions in ionic nanocrystals,” *Science* **306**, 1009–1012 (2004).
- <sup>28</sup>P. Monceau, “Electronic crystals: An experimental overview,” *Advances in Physics* **61**, 325–581 (2012).
- <sup>29</sup>A. E. Hughes and S. C. Jain, “Metal colloids in ionic crystals,” *Advances in Physics* **28**, 717–828 (1979).
- <sup>30</sup>H. Tanaka, Y. Okano, H. Kobayashi, W. Suzuki, and A. Kobayashi, “A three-dimensional synthetic metallic crystal composed of single-component molecules,” *Appl. Phys. Lett* **52**,



- 5098 (1999).
- <sup>31</sup>J. Pistor and C. Körner, “A novel mechanism to generate metallic single crystals,” *Scientific Reports* **11** (2021), 10.1038/s41598-021-04235-2.
- <sup>32</sup>A. L. Rogach, D. V. Talapin, E. V. Shevchenko, A. Kornowski, M. Haase, and H. Weller, “Organization of matter on different size scales: Monodisperse nanocrystals and their superstructures,” *Advanced Functional Material* **12**, 653–664 (2002).
- <sup>33</sup>E. V. Shevchenko, D. V. Talapin, N. A. Kotov, S. O’Brien, and C. B. Murray, “Structural diversity in binary nanoparticle superlattices,” *Nature* **439**, 55–59 (2006).
- <sup>34</sup>M. R. Jones, R. J. MacFarlane, B. Lee, J. Zhang, K. L. Young, A. J. Senesi, and C. A. Mirkin, “Dna-nanoparticle superlattices formed from anisotropic building blocks,” *Nature Materials* **9**, 913–917 (2010).
- <sup>35</sup>Y. Zhang, F. Lu, K. G. Yager, D. V. D. Lelie, and O. Gang, “A general strategy for the dna-mediated self-assembly of functional nanoparticles into heterogeneous systems,” *Nature Nanotechnology* **8**, 865–872 (2013).
- <sup>36</sup>D. Samanta, W. Zhou, S. B. Ebrahimi, S. H. Petrosko, and C. A. Mirkin, “Programmable matter: The nanoparticle atom and dna bond,” *Advanced Materials* **34** (2022), 10.1002/adma.202107875.
- <sup>37</sup>S. Zang, A. W. Hauser, S. Paul, G. M. Hocky, and S. Sacanna, “Enabling three-dimensional real-space analysis of ionic colloidal crystallization,” *Nature Materials* (2024), 10.1038/s41563-024-01917-w.
- <sup>38</sup>P. F. Damasceno, M. Engel, and S. C. Glotzer, “Crystalline assemblies and densest packings of a family of truncated tetrahedra and the role of directional entropic forces,” *ACS Nano* **6**, 609–614 (2012).
- <sup>39</sup>A. P. Gantapara, J. D. Graaf, R. V. Roij, and M. Dijkstra, “Phase diagram and structural diversity of a family of truncated cubes: Degenerate close-packed structures and vacancy-rich states,” *Physical Review Letters* **111**, 1–5 (2013).
- <sup>40</sup>Z. Zhang, A. S. Keys, T. Chen, and S. C. Glotzer, “Self-assembly of patchy particles into diamond structures through molecular mimicry,” *Langmuir* **21**, 11547–11551 (2005).
- <sup>41</sup>D. Chen, G. Zhang, and S. Torquato, “Inverse design of colloidal crystals via optimized patchy interactions,” *Journal of Physical Chemistry B* **122**, 8462–8468 (2018).
- <sup>42</sup>M. N. O’Brien, M. Girard, H. X. Lin, J. A. Millan, M. O. D. L. Cruz, B. Lee, and C. A. Mirkin, “Exploring the zone of anisotropy and broken symmetries in dna-mediated

- nanoparticle crystallization,” *Proceedings of the National Academy of Sciences of the United States of America* **113**, 10485–10490 (2016).
- <sup>43</sup>D. Frenkel and B. M. Mulder, “The hard ellipsoid-of-revolution fluid i. monte carlo simulations,” *Molecular Physics* **55**, 1171–1192 (1985).
- <sup>44</sup>S. C. McGrother, D. C. Williamson, and G. Jackson, “A re-examination of the phase diagram of hard spherocylinders,” *Journal of Chemical Physics* **104**, 6755–6771 (1996).
- <sup>45</sup>P. Bolhuis and D. Frenkel, “Tracing the phase boundaries of hard spherocylinders,” *Journal of Chemical Physics* **106**, 666–687 (1997).
- <sup>46</sup>B. S. John, C. Juhlin, and F. A. Escobedo, “Phase behavior of colloidal hard perfect tetragonal parallelepipeds,” *Journal of Chemical Physics* **128** (2008), 10.1063/1.2819091.
- <sup>47</sup>A. Haji-Akbari, M. Engel, A. S. Keys, X. Zheng, R. G. Petschek, P. Palffy-Muhoray, and S. C. Glotzer, “Disordered, quasicrystalline and crystalline phases of densely packed tetrahedra,” *Nature* **462**, 773–777 (2009).
- <sup>48</sup>P. J. Steinhardt, D. R. Nelson, and M. Ronchetti, “Bond-orientational order in liquids and glasses,” (1983).
- <sup>49</sup>D. Faken and H. Jónsson, “Systematic analysis of local atomic structure combined with 3d computer graphics,” *Computational Materials Science* **2**, 279–286 (1994).
- <sup>50</sup>W. Lechner and C. Dellago, “Accurate determination of crystal structures based on averaged local bond order parameters,” *Journal of Chemical Physics* **129**, 114707 (2008).
- <sup>51</sup>R. V. Damme, G. M. Coli, R. V. Roij, and M. Dijkstra, “Classifying crystals of rounded tetrahedra and determining their order parameters using dimensionality reduction,” *ACS Nano* **14**, 15144–15153 (2020).
- <sup>52</sup>A. D. Kalian, E. Benfenati, O. J. Osborne, D. Gott, C. Potter, J. L. C. Dorne, M. Guo, and C. Hogstrand, “Exploring dimensionality reduction techniques for deep learning driven qsar models of mutagenicity,” *Toxics* **11** (2023), 10.3390/toxics11070572.
- <sup>53</sup>J. D. Honeycutt and H. C. Andersen, “Molecular dynamics study of melting and freezing of small lennard-jones clusters,” *J. Phys. Chem* **91**, 4950–4963 (1987).
- <sup>54</sup>N. Duff and B. Peters, “Polymorph specific rmsd local order parameters for molecular crystals and nuclei: alpha-, beta- and gamma-glycine,” *Journal of Chemical Physics* **135**, 134101 (2011).
- <sup>55</sup>W. F. Reinhart and A. Z. Panagiotopoulos, “Automated crystal characterization with a fast neighborhood graph analysis method,” *Soft Matter* **14**, 6083–6089 (2018).

- <sup>56</sup>C. N. Li, H. P. Liang, X. Zhang, Z. Lin, and S. H. Wei, “Graph deep learning accelerated efficient crystal structure search and feature extraction,” *npj Computational Materials* **9** (2023), 10.1038/s41524-023-01122-4.
- <sup>57</sup>E. Boattini, M. Dijkstra, and L. Filion, “Unsupervised learning for local structure detection in colloidal systems,” *Journal of Chemical Physics* **151**, 154901 (2019).
- <sup>58</sup>M. Spellings and S. C. Glotzer, “Machine learning for crystal identification and discovery,” *AIChE Journal* **64**, 2198–2206 (2018).
- <sup>59</sup>K. Ryan, J. Lengyel, and M. Shatruk, “Crystal structure prediction via deep learning,” *Journal of the American Chemical Society* **140**, 10158–10168 (2018).
- <sup>60</sup>E. Boattini, M. Ram, F. Smalenburg, and L. Filion, “Neural-network-based order parameters for classification of binary hard-sphere crystal structures,” *Molecular Physics* **116**, 3066–3075 (2018).
- <sup>61</sup>M. A. Boles, M. Engel, and D. V. Talapin, “Self-assembly of colloidal nanocrystals: From intricate structures to functional materials,” (2016).
- <sup>62</sup>A. Bhattacharyya, S. C. Makhal, and N. Guchhait, “Chef-affected fluorogenic nanomolar detection of  $\text{Al}^{3+}$  by an anthranilic acid-naphthalene hybrid: Cell imaging and crystal structure,” *ACS Omega* **3**, 11838–11846 (2018).
- <sup>63</sup>L. Rossi, S. Sacanna, W. T. Irvine, P. M. Chaikin, D. J. Pine, and A. P. Philipse, “Cubic crystals from cubic colloids,” *Soft Matter* **7**, 4139–4142 (2011).
- <sup>64</sup>G. V. Anders, D. Klotsa, A. S. Karas, P. M. Dodd, and S. C. Glotzer, “Digital alchemy for materials design: Colloids and beyond,” *ACS Nano* **9**, 9542–9553 (2015).
- <sup>65</sup>J. Dshemuchadse, D. Y. Jung, and W. Steurer, “Structural building principles of complex face-centered cubic intermetallics,” *Acta Crystallographica Section B: Structural Science* **67**, 269–292 (2011).
- <sup>66</sup>P. K. Bommineni, N. R. Varela-Rosales, M. Klement, and M. Engel, “Complex crystals from size-disperse spheres,” *Physical Review Letters* **122** (2019), 10.1103/PhysRevLett.122.128005.
- <sup>67</sup>M. C. Rechtsman, F. H. Stillinger, and S. Torquato, “Self-assembly of the simple cubic lattice with an isotropic potential,” *Physical Review E - Statistical, Nonlinear, and Soft Matter Physics* **74** (2006), 10.1103/PhysRevE.74.021404.
- <sup>68</sup>J. Dshemuchadse, P. F. Damasceno, C. L. Phillips, M. Engel, and S. C. Glotzer, “Moving beyond the constraints of chemistry via crystal structure discovery with isotropic multiwell

- pair potentials,” Proceedings of the National Academy of Sciences of the United States of America **118** (2021), 10.1073/pnas.2024034118/-/DCSupplemental.y.
- <sup>69</sup>J. Dshemuchadse and W. Steurer, “Some statistics on intermetallic compounds,” Inorganic Chemistry **54**, 1120–1128 (2015).
- <sup>70</sup>R. L. Marson, E. G. Teich, J. Dshemuchadse, S. C. Glotzer, and R. G. Larson, “Computational self-assembly of colloidal crystals from platonic polyhedral sphere clusters,” Soft Matter **15**, 6288–6299 (2019).
- <sup>71</sup>U. Agarwal and F. A. Escobedo, “Mesophase behaviour of polyhedral particles,” Nature Materials **10**, 230–235 (2011).
- <sup>72</sup>H. Pan and J. Dshemuchadse, “Targeted discovery of low-coordinated crystal structures via tunable particle interactions,” ACS Nano **17**, 7157–7169 (2023).
- <sup>73</sup>J. Çamkiran, F. Parsch, and G. D. Hibbard, “A local orientational order parameter for systems of interacting particles,” Journal of Chemical Physics **156** (2022), 10.1063/5.0079985.
- <sup>74</sup>H. Eslami, P. Sedaghat, and F. Müller-Plathe, “Local bond order parameters for accurate determination of crystal structures in two and three dimensions,” Physical Chemistry Chemical Physics **20**, 27059–27068 (2018).
- <sup>75</sup>J. A. Logan, A. Michelson, A. Pattammattel, H. Yan, O. Gang, and A. V. Tkachenko, “Symmetry-specific characterization of bond orientation order in dna-assembled nanoparticle lattices,” Journal of Chemical Physics **159** (2023), 10.1063/5.0168604.
- <sup>76</sup>M. Engel, “Point group analysis in particle simulation data,” (2021).
- <sup>77</sup>J. Bernstein, I. G. R. D. Cruickshank, H. Juretschke, N. Kato, R. Snyder, J. Fiala, and H. Bunge, *Crystal Structure Analysis: Principles and Practice (International Union of Crystallography)*, Vol. 2 (2009).
- <sup>78</sup>J. A. Hartigan and M. A. Wong, “A k-means clustering algorithm,” JSTOR: Applied Statistics **28**, 100–108 (1979).
- <sup>79</sup>V. Ramasubramani, B. D. Dice, E. S. Harper, M. P. Spellings, J. A. Anderson, and S. C. Glotzer, “freud: A software suite for high throughput analysis of particle simulation data,” Computer Physics Communications **254**, 107275 (2020).
- <sup>80</sup>P. M. Larsen, S. Schmidt, and J. SchiÖtz, “Robust structural identification via polyhedral template matching,” Modelling and Simulation in Materials Science and Engineering **24** (2016), 10.1088/0965-0393/24/5/055007.

- <sup>81</sup>V. Ramasubramani, B. D. Dice, T. T. Dwyer, and S. C. Glotzer, “coxeter: A python package for working with shapes,” *Journal of Open Source Software* **6**, 3098 (2021).
- <sup>82</sup>P. Virtanen, R. Gommers, T. E. Oliphant, M. Haberland, T. Reddy, D. Cournapeau, E. Burovski, P. Peterson, W. Weckesser, J. Bright, S. J. van der Walt, M. Brett, J. Wilson, K. J. Millman, N. Mayorov, A. R. J. Nelson, E. Jones, R. Kern, E. Larson, C. J. Carey, Í. Polat, Y. Feng, E. W. Moore, J. VanderPlas, D. Laxalde, J. Perktold, R. Cimrman, I. Henriksen, E. A. Quintero, C. R. Harris, A. M. Archibald, A. H. Ribeiro, F. Pedregosa, P. van Mulbregt, and SciPy 1.0 Contributors, “SciPy 1.0: Fundamental Algorithms for Scientific Computing in Python,” *Nature Methods* **17**, 261–272 (2020).
- <sup>83</sup>*International Tables for Crystallography Volume A Space-group symmetry*, 2nd ed. (Wiley, 2016).
- <sup>84</sup>S. Gražulis, A. Daškevič, A. Merkys, D. Chateigner, L. Lutterotti, M. Quirós, N. R. Serebryanaya, P. Moeck, R. T. Downs, and A. L. Bail, “Crystallography open database (cod): An open-access collection of crystal structures and platform for world-wide collaboration,” *Nucleic Acids Research* **40** (2012), 10.1093/nar/gkr900.
- <sup>85</sup>A. Kitano, K. Moriguchi, M. Yonemura, S. Munetoh, A. Shintani, H. Fukuoka, S. Yamana, E. Nishibori, M. Takata, and M. Sakata, “Structural properties and thermodynamic stability of ba-doped silicon type-i clathrates synthesized under high pressure,” *Physical Review B - Condensed Matter and Materials Physics* **64**, 452061–452069 (2001).
- <sup>86</sup>G. Vanhoyland, M. K. V. Bael, J. Mullens, and L. C. V. Poucke, “Structure determination of anhydrous acid strontium oxalate by conventional x-ray powder diffraction,” *Powder Diffraction* **16**, 224–226 (2001).
- <sup>87</sup>M. Miyake, H. Morikawa, and S.-I. Iwai, “Structure reinvestigation of the high-temperature form of k<sub>2</sub>so<sub>4</sub>,” *Acta Cryst. B* **36**, 532–536 (1980).
- <sup>88</sup>Y. Wang, I. C. Jenkins, J. T. McGinley, T. Sinno, and J. C. Crocker, “Colloidal crystals with diamond symmetry at optical lengthscales,” *Nature Communications* **8** (2017), 10.1038/ncomms14173.
- <sup>89</sup>D. Klotsa, E. R. Chen, M. Engel, and S. C. Glotzer, “Intermediate crystalline structures of colloids in shape space,” *Soft Matter* **14**, 8692–8697 (2018).
- <sup>90</sup>G. J. Ackland and A. P. Jones, “Applications of local crystal structure measures in experiment and simulation,” *Physical Review B - Condensed Matter and Materials Physics* **73**, 10.1103/PhysRevB.73.054104.

<sup>91</sup>G. H. Fecher, J. Kübler, and C. Felser, “Chirality in the solid state: Chiral crystal structures in chiral and achiral space groups,” *Materials* **15** (2022), 10.3390/ma15175812.